Biochemical Journal (2020) **477** 1499–1513
https://doi.org/10.1042/BCJ20190873

PORTLAND PRESS

Research Article

Hereditary hemochromatosis disrupts uric acid homeostasis and causes hyperuricemia via altered expression/activity of xanthine oxidase and ABCG2

Bojana Ristic, Sathish Sivaprakasam, Monisha Narayanan and Vadivel Ganapathy

Department of Cell Biology and Biochemistry, Texas Tech University Health Sciences Center, Lubbock, TX 79430, U.S.A.

Correspondence: Vadivel Ganapathy (vadivel.ganapathy@ttuhsc.edu)

Hereditary hemochromatosis (HH) is mostly caused by mutations in the iron-regulatory gene *HFE*. The disease is associated with iron overload, resulting in liver cirrhosis/cancer, cardiomegaly, kidney dysfunction, diabetes, and arthritis. Fe^{2+}-induced oxidative damage is suspected in the etiology of these symptoms. Here we examined, using $Hfe^{-/-}$ mice, whether disruption of uric acid (UA) homeostasis plays any role in HH-associated arthritis. We detected elevated levels of UA in serum and intestine in $Hfe^{-/-}$ mice compared with controls. Though the expression of xanthine oxidase, which generates UA, was not different in liver and intestine between wild type and $Hfe^{-/-}$ mice, the enzymatic activity was higher in $Hfe^{-/-}$ mice. We then examined various transporters involved in UA absorption/excretion. Glut9 expression did not change; however, there was an increase in Mrp4 and a decrease in Abcg2 in $Hfe^{-/-}$ mice. As ABCG2 mediates intestinal excretion of UA and mutations in ABCG2 cause hyperuricemia, we examined the potential connection between iron and ABCG2. We found p53-responsive elements in h*ABCG2* promoter and confirmed with chromatin immunoprecipitation that p53 binds to this promoter. p53 protein was reduced in $Hfe^{-/-}$ mouse intestine. p53 is a heme-binding protein and p53-heme complex is subjected to proteasomal degradation. We conclude that iron/heme overload in HH increases xanthine oxidase activity and also promotes p53 degradation resulting in decreased ABCG2 expression. As a result, systemic UA production is increased and intestinal excretion of UA via ABCG2 is decreased, causing serum and tissue accumulation of UA, a potential factor in the etiology of HH-associated arthritis.

Introduction

Uric acid (UA), the ubiquitous end-product of purine catabolism, is an intriguing molecule whose biochemical and pathological effects are dictated by its concentration and the surrounding microenvironment. UA is one of the major endogenous antioxidants whose action is directed towards prevention of lipid peroxidation and inactivation of nitric oxide synthase [1]. In addition, UA is a potent iron chelator; it minimizes iron-mediated redox reactions and generation of reactive oxygen species (ROS) [2]. However, this is true only when UA is present in physiologic concentrations, which is 3.5–7.2 mg/dl in adult males and postmenopausal females and 2.6–6.0 mg/dl in premenopausal women [3]. However, the antioxidant capacity of UA is overshadowed by detrimental effects when its concentration exceeds its maximal solubility (6–7 mg/dl) [4]. In this scenario, UA precipitates and crystalizes as monosodium urate (MSU), which gets deposited in joints, leading to inflammation and gouty arthritis [5]. Since there is an overlap in UA concentrations that define hyperuricemia and that dictate MSU crystal formation, and both have pathological implications, recent discussions continue to emphasize the need for reduction in this 'healthy' UA range [3].

Received: 27 November 2019
Revised: 30 March 2020
Accepted: 1 April 2020

Accepted Manuscript online: 2 April 2020
Version of Record published: 29 April 2020

Biochemical Journal (2020) 477 1499–1513
https://doi.org/10.1042/BCJ20190873

Origin of inflammation caused by MSU crystals is multifactorial. MSU crystals in synovium are engulfed by neutrophils/monocytes where they initiate ROS production and cell death [5]. In addition, they communicate with resident macrophages; upon encounter, MSU crystals trigger the assembly of NLRP3-inflammasome in macrophages and stimulate production and secretion of the proinflammatory cytokine interleukin-1β [5]. Ultimately, the proinflammatory cytokine storm, accumulation of ROS, and acute (later chronic) flares and excruciating joint pain constitute the pathophysiology of gout [4]. The levels of UA in circulation are dictated by the balance between the rate of its production and the rate of its excretion, and genetics is an important determinant in this phenomenon. Recently we reviewed the genetic defects in various transporters that play a critical role in UA homeostasis, consequently leading to either hypouricemia or hyperuricemia [6].

An additional risk factor for arthritis is iron [7] because free iron participates in redox reactions by acting as an electron donor and receptor, ultimately leading to production of hydroxyl radicals and oxidative damage [8]. If that occurs in synovium, arthritis-like symptoms appear [9,10]. Hereditary hemochromatosis (HH) is considered to be the most prevalent disease associated with iron overload; it affects 1 in 250 individuals in certain populations [11]. It is usually referred to as a 'silent disease' because iron loading and iron-elicited damages occur gradually, and detrimental symptoms appear only at 50–60 years of age [12]. In ∼80% of cases, HH is caused by autosomal recessive mutations in *HFE* gene, with C282Y being the most prevalent mutation [13]. HFE, a major histocompatibility class-I-like plasma membrane protein [14], is a critical component of iron-sensing and iron homeostasis-regulatory complex. Its action is mediated by promotion of the synthesis of hepcidin, a hepatic hormone that regulates the amount of iron that enters circulation from diet and tissue-resident macrophages [15]. Missense mutations in *HFE* disrupt the iron-sensing complex and leads to ablation of hepcidin production [16]; this causes systemic iron overload and iron deposition in multiple organs [17]. As a result of iron deposition and iron-induced oxidative damage, the disease manifests with dysfunction of multiple organs, causing liver cirrhosis and liver cancer, nephropathy, cardiomegaly, diabetes, and pituitary insufficiency.

Arthropathy is commonly seen in patients with HH [18–23]. Iron accumulation and consequent oxidative damage are believed to be the principal cause of joint damage in HH. Calcium pyrophosphate dihydrate crystals are found in affected joints, imitating pseudogout [24] and free iron reduces the clearance of these deposits from joints [25]. There are no published reports linking HH to dysregulation of UA homeostasis; this is intriguing given the well-established role of excess UA in arthritis. This critical knowledge gap renders our current understanding of arthropathy in HH incomplete. Therefore, we examined UA status in HH using a mouse model of HH, namely $Hfe^{-/-}$ mouse. These studies demonstrate that $Hfe^{-/-}$ mice have hyperuricemia and that decreased excretion of UA in the intestine via down-regulation of the UA exporter ABCG2 is likely to be the principal contributor to this phenomenon.

Materials and methods

Animals

$Hfe^{-/-}$ mice on C57BL/6 background were purchased from Jackson Laboratory (Bar Harbor, ME, U.S.A.) and C57BL/6 $Abcg2^{-/-}$ mice were purchased from University of California Davis Knockout Mouse Project (KOMP) Repository (Davis, CA, U.S.A.). The mice were maintained at the animal facility of Texas Tech University Health Sciences Center (TTUHSC) in a temperature- and light-controlled environment, with water and laboratory rodent diet provided ad-libitum. Male and female mice older than 7 months were used in this study. The control mice matched the background strain, age and gender of the experimental groups. All experimental procedures were approved by the TTUHSC Institutional Animal Care and Use Committee (IACUC—protocol number 18005) and the Institutional Review Board (IRB). For tissue collection, mice were killed by cervical dislocation under CO_2 anesthesia in accordance with the guidelines from the American Veterinary Medical Association.

Cell culture

Normal human colonic epithelial cell line, CCD841, was purchased from American Type Culture Collection (ATCC, Manassas, VA, U.S.A.). The cell line was cultured in RPMI 1640 (Corning, Corning, NY, U.S.A.) supplemented with 10% FBS (Fisher Scientific, Pittsburgh, PA, U.S.A.) and 1% penicillin/streptomycin (Corning, Corning, NY, U.S.A.). Viral packaging cell line, HEK293FT, was purchased from ATTC (Manassas, VA, U.S.A.) and maintained in DMEM 4.5 g/L glucose, L-glutamine, sodium pyruvate (Corning, Corning, NY, U.S.A.) supplemented with 10% FBS and 1% penicillin/streptomycin. HEK293FT cells were used for transient transfection

experiments where they were cultured for three passages in the presence and absence of excess iron in the form of ferric ammonium citrate (FAC) (Sigma, St. Louis, MO, U.S.A.) [26] and then used for ectopic expression of p53.

Antibodies

Anti-ABCG2 (D5V2K XP®, #42078) and anti-p53 (1C12, #2524) monoclonal antibodies were purchased from Cell Signaling Technology (Danvers, MA, U.S.A.). Anti-β-actin (C4, sc-47778) and anti-β-tubulin (D-10, sc-5274) monoclonal antibodies were purchased from Santa Cruz Biotechnology (Dallas, TX, U.S.A.). Anti-xanthine oxidase monoclonal antibody (EPR4605, ab109235) was purchased from Abcam (Cambridge, MA, U.S.A.) and anti-GLUT9 polyclonal antibody (PA5-22966) was purchased from Thermo Fisher Scientific (Waltham, MA, U.S.A.). Horseradish peroxidase-conjugated goat anti-rabbit (#1706515) and goat anti-mouse (#1706516) were purchased from Bio-Rad Laboratories (Hercules, CA, U.S.A.).

Measurement of UA

The UA content of the intestinal tissue and serum was measured by the fluorimetry-based Uric Acid Assay Kit (Abcam, Cambridge, MA, U.S.A.), as described by the manufacturer. The UA concentration of the tissue was recorded as nmol of UA per milligram of protein, while the serum concentration was recorded as nmol of UA per ml of serum.

Measurement of serum creatinine

Creatinine concentration in serum was measured by the fluorimetry-based Creatinine Assay Kit (Biovision, Milpitas, CA, U.S.A.) as per manufacturer's protocol. The creatinine concentration was recorded as mg/dl of serum.

Measurement of uricase activity

Uricase activity in liver and colon was measured by the fluorimetry-based Amplex® Red Uric Acid/Uricase Assay Kit (Thermo Fisher Scientific, Waltham, MA, U.S.A.) as per manufacturer's protocol. Uricase activity was recorded as mU/mg protein. One unit is defined as the amount of enzyme that will convert 1 μmole of uric acid to allantoin per min at pH 8.5 and 25°C.

Measurement of XO activity

XO activity in liver and jejunum was measured by fluorimetry-based XO Activity Assay Kit (Sigma, St. Louis, MO, U.S.A.) as per manufacturer's protocol. XO activity was recorded as nmol of H_2O_2 generated per minute per milligram of protein.

RNA isolation and quantitative PCR

Total RNA from animal tissues and cultured cells was extracted using TRIzol reagent (Thermo Fisher Scientific, Waltham, MA, U.S.A.). RNA purity and concentration were quantified using NanoDrop Spectrophotometer 2000 (Thermo Fisher Scientific, Waltham, MA, U.S.A.). An amount of 2 μg of RNA was reverse transcribed into cDNA using the SuperScript III First-Strand cDNA synthesis kit (Thermo Fisher Scientific, Waltham, MA, U.S.A.). Relative mRNA levels were measured with StepOne Plus real-time PCR system (Applied Biosystems, Foster City, CA, U.S.A.) using the SYBR® Green supermix (Bio-Rad Laboratories, Hercules, CA, U.S.A.), and were normalized to the housekeeping gene HGPRT (hypoxanthine/guanine phosphoribosyl transferase). The PCR primer sequences are given in Supplementary Table S1.

Protein isolation and Western blot

For whole tissue/cell extract preparation, tissues and cells were lysed in Pierce™ RIPA buffer (Thermo Fisher Scientific, Waltham, MA, U.S.A.) supplemented with Halt™ Protease and Phosphatase Inhibitor Cocktail (Thermo Fisher Scientific, Waltham, MA, U.S.A.). Homogenates were centrifuged, and supernatants were used for protein measurement via Pierce™ BCA Protein Assay Kit (Thermo Fisher Scientific, Waltham, MA, U.S.A.). Western blot samples were prepared in Laemmli Sample Buffer (Bio-Rad Laboratories, Hercules, CA, U.S.A.). They were loaded onto a 10% SDS–polyacrylamide gel electrophoresis (SDS–PAGE) gel and transferred onto a PVDF membrane (Bio-Rad Laboratories, Hercules, CA, U.S.A.). The membrane was blocked, and antibodies diluted in 5% nonfat dry milk (Bio-Rad Laboratories, Hercules, CA, U.S.A.) or in 5% bovine serum albumin

Biochemical Journal (2020) 477 1499–1513
https://doi.org/10.1042/BCJ20190873

(Irvine Scientific, Santa Ana, CA, U.S.A.) were used. Protein bands were visualized using Pierce™ ECL Western Blotting Substrate (Thermo Fisher Scientific, Waltham, MA, U.S.A.) and developed on the autoradiography film (Santa Cruz, Dallas, TX, U.S.A.).

Isolation of ileal and colonic mucosal epithelial cells

Ileum and colon were cut open longitudinally, washed with ice-cold phosphate-buffered saline and placed on an ice-cold glass surface with the lumen side facing up. The epithelium was mechanically detached and collected by scraping with the glass slide. Samples were centrifuged and the pellet was used for further analysis.

Lentiviral transfection

Construct for shRNA to degrade p53 mRNA (pLKO-p53-shRNA-427; Addgene plasmid # 25636) was created by Todd Waldman laboratory and purchased from Addgene plasmid repository (Watertown, MA, U.S.A.) [27]. pLKO.1 empty vector was used as a control. To generate transient virus stock, HEK293FT cells were plated in 10-cm dish and allowed to reach 100% confluency. An amount of 7.5 μg of control, shRNA vector, and packaging plasmids (PLP1, PLP2, and VSVG) were delivered to the cells using Lipofectamine-2000 reagent (Thermo Fisher Scientific, Waltham, MA, U.S.A.). Forty-eight hours after transient transfection, the virus-containing medium was harvested, centrifuged and filtered to generate virus stock. CCD841 cells were seeded in six-well plates; they were at 50% confluency on the day of the infection. Virus stock contained 8 μg/ml of polybrene to increase the transduction efficacy. Forty-eight hours after infection, desired clones were selected by administration of puromycin (1 μg/ml).

Chromatin immunoprecipitation assay

ChIP assays were performed using EZ-Magna ChIP A/G kit (Millipore, Burlington, MA, U.S.A.) according to the manufacturer's instructions. Briefly, cells were cross-linked with 1% formaldehyde, collected in phosphate-buffered saline supplemented with Halt™ Protease and Phosphatase Inhibitor Cocktail (Thermo Fisher Scientific, Waltham, MA, U.S.A.) and lysed in nuclear lysis buffer. The lysate was then sonicated using BioRuptor Plus (Diagenode, Denville, NJ, U.S.A.) to shear DNA into fragments of ∼200–1000 base pairs. DNA concentration was measured using NanoDrop Spectrophotometer 2000 (Thermo Fisher Scientific, Waltham, MA) and 25 μg of DNA was used for immunoprecipitation with anti-p53 antibody or normal mouse IgG. Before immunoprecipitation, 1% of the supernatant was removed as an input. DNA was isolated on the column and relative enrichment of p53 on h*ABCG2* gene promoter was assessed via real-time quantitative PCR. The PCR primer sequences are provided in Supplementary Table S1.

Transient transfection

Construct for wild-type p53 (pcDNA3 p53 WT; Addgene plasmid # 69003) was purchased from Addgene plasmid repository (Watertown, MA, U.S.A.) [28]. pcDNA3 empty vector was used as a control. HEK293FT cells were cultured first for three passages in the absence or presence of FAC (250 μg/ml) and then used for transient ectopic expression of p53. Control and iron-overloaded cells were plated in six-well plates and allowed to reach 80–90% confluency. An amount of 2.5 μg of control and p53 WT plasmids were delivered to the cells using Lipofectamine-3000 reagent (Thermo Fisher Scientific, Waltham, MA, U.S.A.). Ferric ammonium citrate was absent during the transfection step, but was added to the culture medium after that step. Forty-eight hours 48 h later, RNA and protein lysates were prepared.

Statistical analysis

Experiments were repeated at least three times. The data shown are representative results of the means ± SEM. Statistical analyses and graphing were performed using GraphPad Prism 7.01 software. Statistical differences between control and experimental groups were analyzed by a two-tailed, unpaired Student's *t*-test for single comparison. Differences were judged statistically significant when the P value <0.05.

Results

Hfe$^{-/-}$ mouse exhibits hyperuricemia

To assess if HH leads to the development of hyperuricemia, we measured systemic and organ-specific UA concentration in *Hfe*$^{-/-}$ mice. We found that, when compared with the wild type, *Hfe*$^{-/-}$ mice had elevated UA in

Biochemical Journal (2020) **477** 1499–1513
https://doi.org/10.1042/BCJ20190873

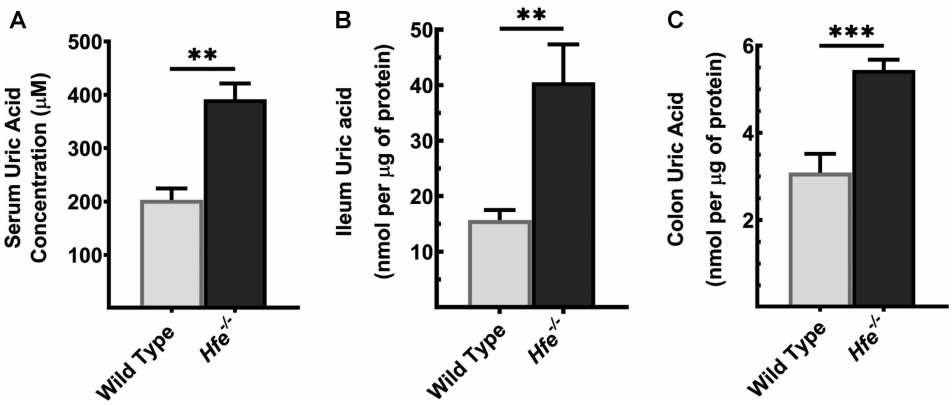

Figure 1. Systemic and organ-specific accumulation of UA in *Hfe*$^{-/-}$ mice.

UA concentration was measured in (**A**) serum, (**B**) ileum, and (**C**) colon in *Hfe*$^{-/-}$ mice and their wild-type counterparts using UA Assay Kit. Mice used in the study were 14-months old. Data show mean values of three mice per group ± SEM. $^{**}P < 0.01$, $^{***}P < 0.001$.

the circulation (Figure 1A). As the large intestine and mid-to-distal parts of the small intestine are involved in UA homeostasis, contributing to at least 40% to total UA excretion, we monitored UA levels in *Hfe*$^{-/-}$ intestine. Compared with the control, *Hfe*$^{-/-}$ ileum (Figure 1B) and colon (Figure 1C) had a significantly higher accumulation of UA.

Besides the intestinal tract, UA is excreted by the kidneys [29]; as such, renal dysfunction is also a significant determinant of circulating levels of UA. Therefore, we investigated if the observed UA accumulation in serum was due to the impaired glomerular filtration in HH. We estimated the glomerular filtration rate in wild-type mice and *Hfe*$^{-/-}$ mice in an indirect manner by measuring the concentration of creatinine in circulation. If the body weight is comparable between the two groups, creatinine levels in blood serve as a surrogate for glomerular filtration rate. For this, we used only male mice; mice in both genotype groups had comparable body weight (Supplementary Figure S1A). We found that the serum creatinine levels did not differ between the two groups (Supplementary Figure S1B), suggesting that there is no difference in glomerular filtration rate between wild type and *Hfe*$^{-/-}$ mice (males, 7-month-old).

Uricase expression and activity in wild type and *Hfe*$^{-/-}$ mice

The hyperuricemia in *Hfe*$^{-/-}$ mice can be due to overproduction, degradation, or underexcretion of UA, or a combination of some or all. To discern the underlying mechanism of UA elevation, we first investigated the expression and activity of uricase (also called urate oxidase), an enzyme that oxidizes UA into allantoin in rodents, but is absent from humans and other higher primates due to the non-functional pseudogene [30]. Quantitative PCR analyses showed no significant difference in the mRNA expression of uricase between two genotypes (Supplementary Figure S2A). In addition, deletion of *Hfe* gene did not alter uricase activity (Supplementary Figure S2B).

Increased enzymatic activity of xanthine oxidase in *Hfe*$^{-/-}$ mouse

Next, we investigated the expression levels and the activity of xanthine oxidase (XO), the enzyme that catalyzes the terminal reaction in UA synthesis [31]. XO is expressed in mouse liver and small intestine, with the highest levels present in jejunum (Figure 2A). On the protein level, however, XO was most abundant in liver; its levels were much less in the intestinal tract and it decreased aborally (Figure 2B). This expression pattern did not differ between wild type and *Hfe*$^{-/-}$ mice, except for liver, where XO mRNA decreased in *Hfe*$^{-/-}$ mice (Figure 2C,D). Since XO active site contains molybdenum and iron as cofactors [32], we pondered whether excess iron alters XO enzyme activity. We measured XO enzymatic activity in liver and jejunum of wild type and *Hfe*$^{-/-}$ mice. We found a significant increase in XO activity in *Hfe*$^{-/-}$ liver and jejunum (Figure 2E).

Biochemical Journal (2020) **477** 1499–1513
https://doi.org/10.1042/BCJ20190873

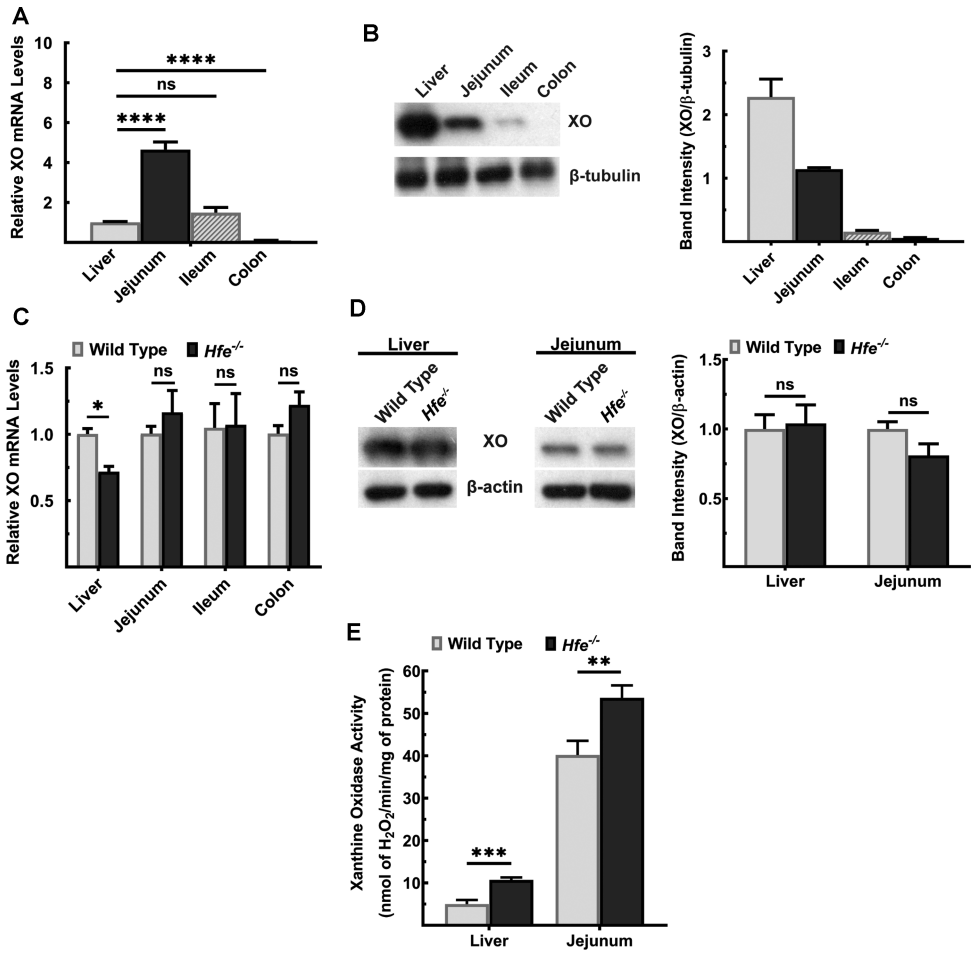

Figure 2. Activity of XO, but not its expression, is significantly increased in *Hfe*$^{-/-}$ mouse liver and small intestine.

(**A**) Quantitative PCR analysis of XO mRNA in liver and intestinal segments of wild-type mouse. Data show mean values ± SEM relative to liver, which is taken as 1. ****$P < 0.0001$; ns, not significant. (**B**) Western blot for XO protein levels in liver and intestinal segments of wild-type mouse. Western blot band intensities were estimated using ImageJ software and the band intensities were normalized to the respective β-tubulin band intensities. Please see Supplementary Figures S4 and S5 for full blot images. (**C**) Quantitative PCR analysis of XO mRNA in liver, jejunum, ileum, and colon of *Hfe*$^{-/-}$ mice and wild-type mice. Data show mean values of three mice per group ± SEM relative to control mice. *$P < 0.05$. (**D**) Western blot for XO protein levels in *Hfe*$^{-/-}$ and wild-type liver and jejunum. Western blot band intensities were estimated using ImageJ software and the band intensities were normalized to the respective β-actin band intensities. Please see Supplementary Figure S6–S9 for full blot images. (**E**) XO activity in wild type and *Hfe*$^{-/-}$ mice. Data show the mean of three mice per group ± SEM. **$P < 0.01$; ***$P < 0.001$.

Glut9 and Mrp4 expression in *Hfe*$^{-/-}$ mouse

We then monitored the expression levels of the transporters that are involved in absorption and excretion of UA in liver and intestine in wild type and *Hfe*$^{-/-}$ mice. We first focused on two transporters: a passive, bidirectional UA carrier GLUT9 (also known as SLC2A9) and an ATP-dependent unidirectional UA exporter MRP4 (ABCC4). These transporters are expressed on apical and basolateral membranes in hepatocytes and enterocytes [33]. Glut9 mRNA expression was comparable between liver and jejunum of the wild-type mice, but it was significantly lower in ileum and colon (Figure 3A). On the contrary, protein levels differed significantly, with Glut9 primarily detectable in the intestinal tract (Figure 3B). More relevant to the current study is the finding that deletion of *Hfe* did not influence the levels of Glut9 mRNA or protein (Figure 3C,D). Mrp4 was expressed highly in liver and colon; its expression increased aborally in the intestinal tract (Figure 3E). When

Biochemical Journal (2020) **477** 1499–1513
https://doi.org/10.1042/BCJ20190873

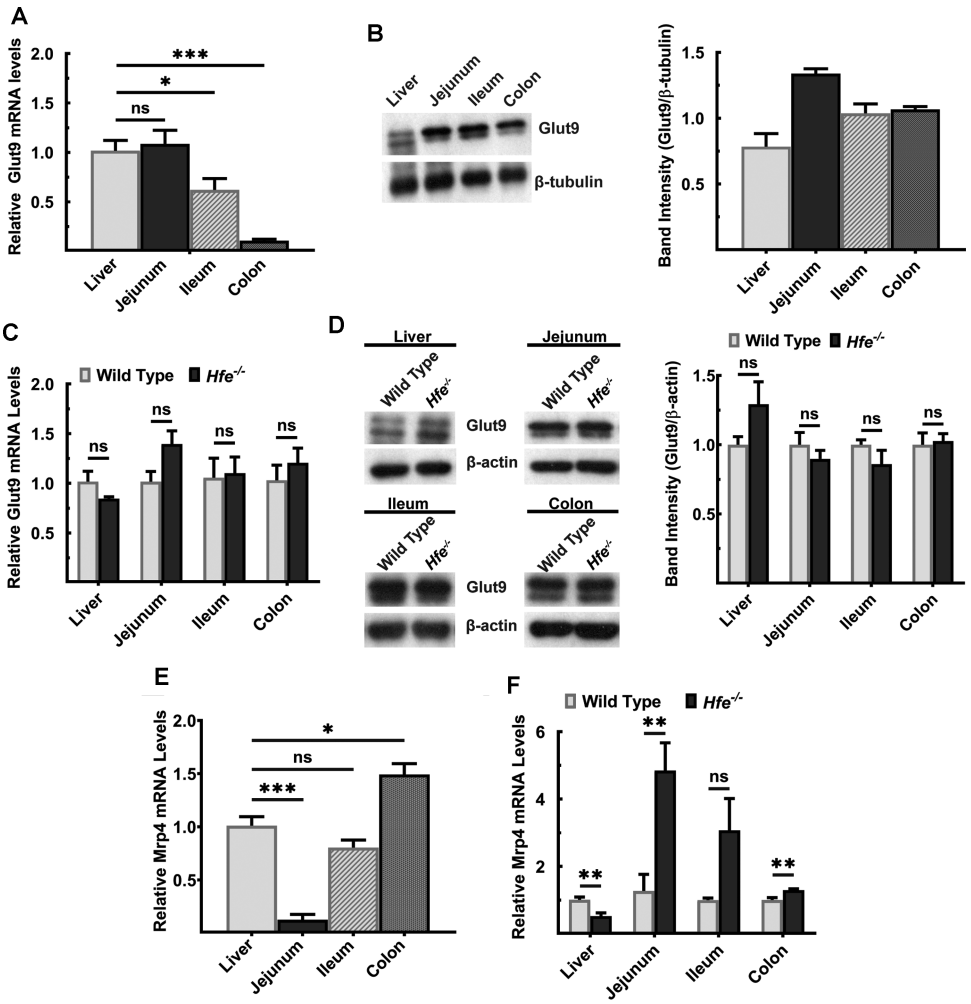

Figure 3. Expression of Glut9 and MRP4 in wild type and *Hfe*$^{-/-}$ mouse liver and intestinal tract.

(**A**) Quantitative PCR analysis of Glut9 mRNA in liver and intestinal segments of wild-type mouse. Data show mean values ± SEM relative to liver, which is taken as 1. *$P < 0.05$; ***$P < 0.001$. (**B**) Western blot for Glut9 protein levels in liver and intestinal segments of the wild-type mouse. Western blot band intensities were estimated using ImageJ software and the band intensities were normalized to the respective β-tubulin band intensities. Please see Supplementary Figures S5 and S10 for full blot images. (**C**) Quantitative PCR of Glut9 mRNA in liver, jejunum, ileum, and colon of *Hfe*$^{-/-}$ mice and wild-type mice. Data show mean values of three mice per group ± SEM relative to control mice. (**D**) Western blot for Glut9 protein levels in *Hfe*$^{-/-}$ mouse and wild-type mouse liver, jejunum, ileum, and colon. Western blot band intensities were estimated using ImageJ software and the band intensities were normalized to the respective β-actin band intensities. Please see Supplementary Figures S8, S9, and S11 for full blot images. (**E**) Quantitative PCR analysis of Mrp4 mRNA in liver and intestinal segments of wild-type mouse. Data show mean values ± SEM relative to liver, which is taken as 1. *$P < 0.05$; ***$P < 0.001$. (**F**) Quantitative PCR analysis of Mrp4 mRNA in liver, jejunum, ileum, and colon of *Hfe*$^{-/-}$ mice and wild-type mice. Data show mean values of three mice per group ± SEM relative to control mice. **$P < 0.01$.

compared with wild-type mice, Mrp4 mRNA levels were lower in the liver, but significantly higher in the jejunum and colon of *Hfe*$^{-/-}$ mice (Figure 3F).

Abcg2 expression in wild-type mouse and impact of *Abcg2* deletion on UA in circulation

UA is a substrate for the ATP-dependent export pump ABCG2 [34]; the transporter is responsible for most of intestinal excretion of UA. Abcg2 mRNA was found in kidney, liver and intestinal tract, highest level of

Biochemical Journal (2020) **477** 1499–1513
https://doi.org/10.1042/BCJ20190873

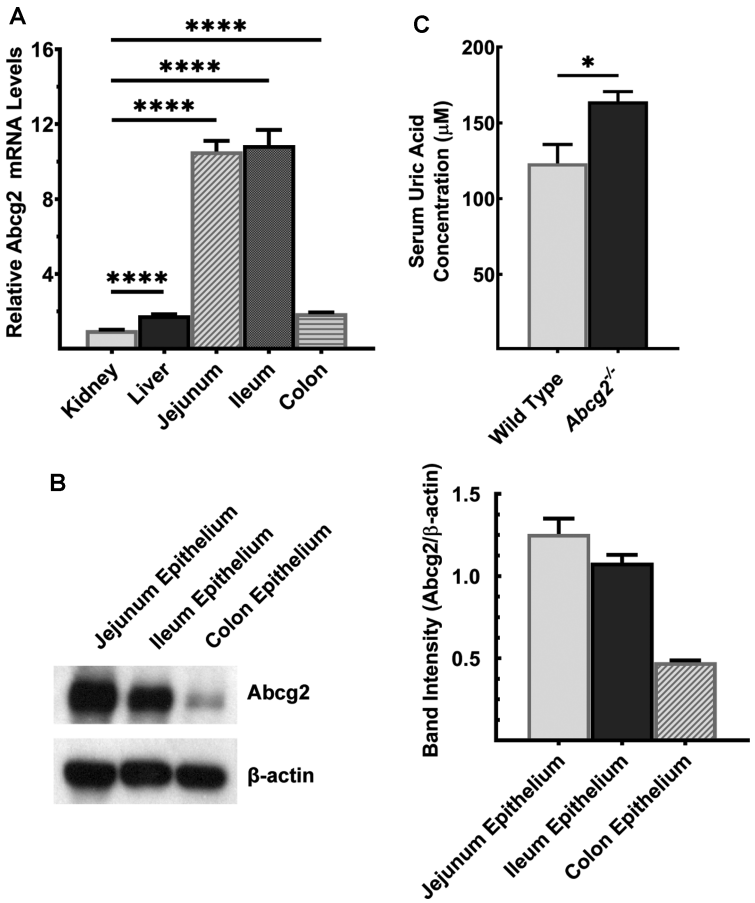

Figure 4. Abcg2 is robustly expressed in mouse intestine.

(**A**) Quantitative PCR analysis of Abcg2 mRNA in kidney, liver, and intestinal segments of wild-type mouse. Data show mean values ± SEM relative to kidney, which is taken as 1. ****$P < 0.0001$. (**B**) Western blot for Abcg2 protein levels in intestinal segments of wild-type mouse. Western blot band intensities were estimated using ImageJ software and the band intensities were normalized to the respective β-actin band intensities. Please see Supplementary Figure S12 for a full blot image. (**C**) UA was measured in serum of *Abcg2*$^{-/-}$ mice and wild-type mice. Mice used in the study were 7-months old. Data show mean values of three mice per group ± SEM. *$P < 0.05$.

expression noted in jejunum and ileum (Figure 4A). Abcg2 protein was highest in jejunum, and it decreased in the intestinal tract aborally (Figure 4B). In a genome-wide association study, Woodward et al. [35] identified multiple SNPs in *ABCG2* to be associated with hyperuricemia and gout. The Q141K mutation decreases the transport function of ABCG2 by ∼50% [35]. This phenomenon is phenocopied in *Abcg2*$^{-/-}$ mice, where complete deletion of *Abcg2* gene resulted in elevated UA levels in circulation (Figure 4C).

Down-regulation of Abcg2 in the intestinal tract of *Hfe*$^{-/-}$ mice

As hyperuricemia was found in *Hfe*$^{-/-}$ mice as well as in *Abcg2*$^{-/-}$ mice, we became curious about a possible connection between HFE and ABCG2. We hypothesized that Abcg2 expression is decreased in HH, thus providing a molecular basis of hyperuricemia in *Hfe*$^{-/-}$ mice. To test this hypothesis, we monitored the expression levels of Abcg2 mRNA and protein in ileum and colon between wild type and *Hfe*$^{-/-}$ mice, specifically in the mucosal epithelium. Abcg2 mRNA was significantly lower in *Hfe*$^{-/-}$ colon (Figure 5A). The Abcg2 protein levels were also lower in ileum and colon in *Hfe*$^{-/-}$ mice (Figure 5B–D). The decrease was ∼5-fold in ileum and ∼3-fold in colon.

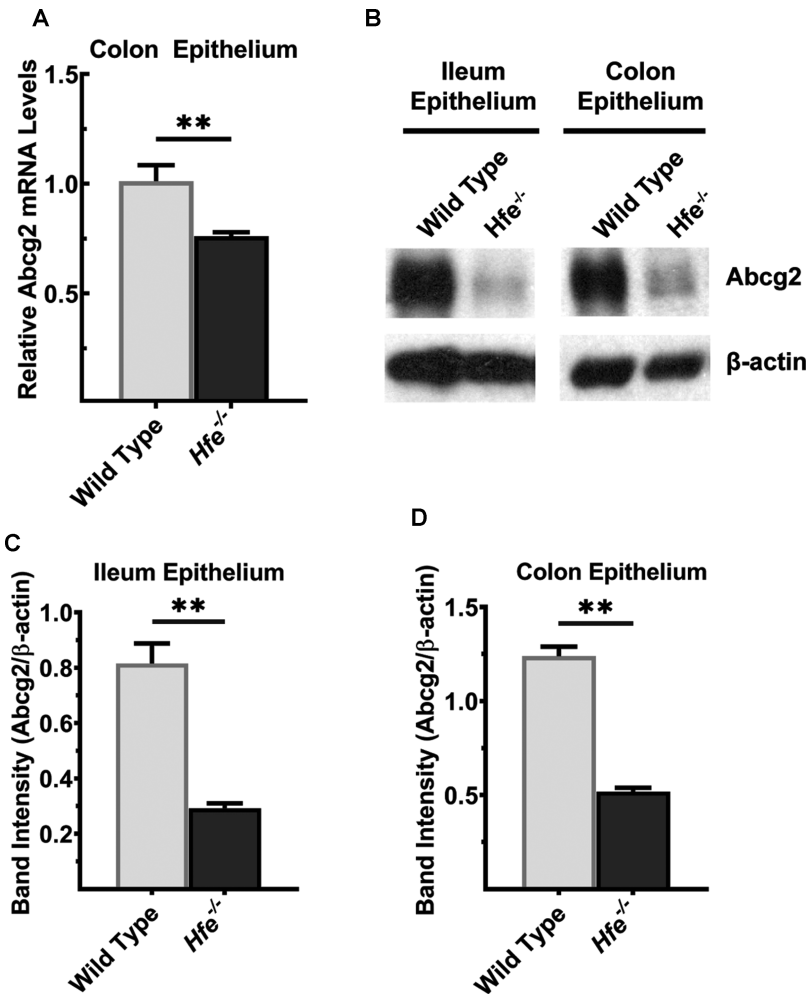

Figure 5. Abcg2 is down-regulated in *Hfe*$^{-/-}$ mouse intestine.

(**A**) Quantitative PCR analysis of Abcg2 mRNA in colon epithelium of *Hfe*$^{-/-}$ mice and wild-type mice. Data show mean values of three mice per group ± SEM relative to control mice. $^{**}P < 0.01$. (**B**) Western blot for Abcg2 protein levels in ileal and colonic epithelium from wild type and *Hfe*$^{-/-}$ mice. Please see Supplementary Figures S13 and S14 for full blot images. Western blot band intensities were estimated using ImageJ software and the band intensities that correspond to the Abcg2 protein were normalized to the respective β-actin levels in (**C**) ileal epithelium and (**D**) colonic epithelium. Data represent mean values of three mice per group ± SEM. $^{**}P < 0.01$.

p53-mediated transcriptional regulation of ABCG2

The follow-up question that needed to be answered was: what is the mechanism underlying the Abcg2 down-regulation in HH mouse? 5′-UTR of h*ABCG2* and m*Abcg2* is located in exon1 and is alternatively spliced to translation start site in exon 2. There are at least 3 splice variants found in both species, which results from alternative promoter usage [36]. Colon h*ABCG2* expresses all three isoforms [37], while m*Abcg2* variants are primarily investigated in hematopoietic stem cells [38]. Analysis of the 5′-UTRs of human *ABCG2* and mouse *Abcg2* 5′ revealed binding sites for p53 (Figure 6A). To test if the interaction between *ABCG2* promoter and p53 occurs in cells, we performed ChIP assay. Experiment was conducted in the normal human colonic epithelial cell line, CCD841. We generated lentiviral transfectants to silence p53 via shRNA, while empty vector was used as a control; we noted a marked decrease in ABCG2 protein levels when p53 was silenced (Figure 6B). If p53 binds to *ABCG2* promoter, the contact between the protein and the promoter would be lower in the shRNA-silenced cell line. We used a specific antibody to pull down p53, and performed quantitative PCR using primers specific for the h*ABCG2* promoter with p53 pulldown. This analysis revealed significant enrichment of

Biochemical Journal (2020) **477** 1499–1513
https://doi.org/10.1042/BCJ20190873

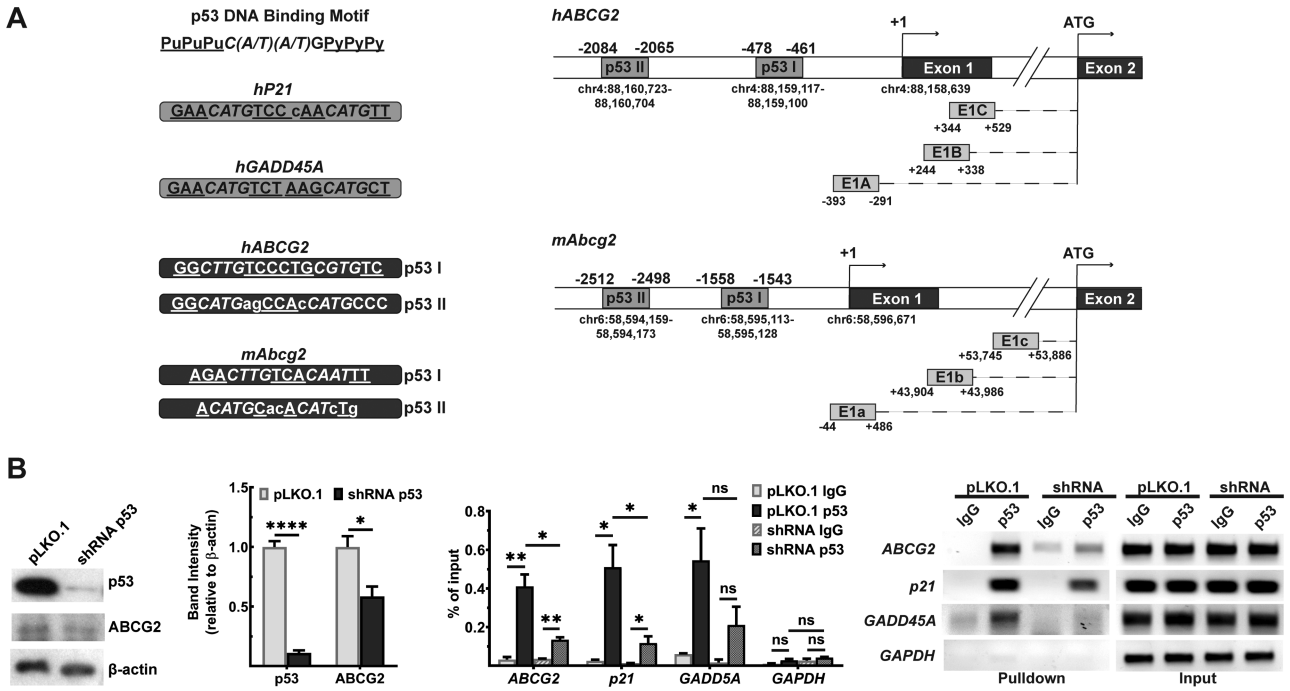

Figure 6. ChIP analysis of p53 binding to human *ABCG2* gene promoter.

(**A**) p53 consensus sequences in h*ABCG2* and m*Abcg2* gene promoters as assessed with JASPAR software. A putative transcription start site (+1) was recognized at the start of the exon 1. Chromosomal locations for this transcription start site and also for p53 consensus sequences are shown. E1A or E1a, E1B or E1b, and E1C or E1c depict the transcript splice variants found in human ABCG2 gene or mouse Abcg2 gene, which result from the alternative promoter usage. (**B**) ChIP analysis for binding of p53 to the h*ABCG2* promoter. Experiment was performed in normal human epithelial cell line CCD841 transfected with either empty vector (pLKO.1) or a vector containing shRNA that targets p53 mRNA. shRNA efficiency was estimated by observing p53 protein levels via Western blot. Please see Supplementary Figures S15–S21 for full blot and agarose gel images. Data show the mean values of three independent experiments ± SEM. $^{*}P < 0.05$; $^{**}P < 0.01$.

ABCG2 promoter in the p53 pulldown. The opposite trend was observed in the shRNA-silenced cell line. When p53 protein levels were lowered, the enrichment was significantly reduced (Figure 6B). The validity and dependability of the method were supported by observations that the pulldown of the p21 and GADD45A, the prototypical targets for p53, was also decreased in cells where p53 was silenced (Figure 6B).

Recent studies have shown that p53 is a heme-binding protein and that p53-heme complex is exported out of nucleus for subsequent proteasomal degradation [39]. This suggested that heme accumulation as occurs in HH might lead to down-regulation of p53 in $Hfe^{-/-}$ mice. Therefore, we hypothesized that decreased expression of p53 is responsible for decreased expression of Abcg2 in $Hfe^{-/-}$ mice. We collected ileal and colonic mucosa of wild type and $Hfe^{-/-}$ mice and performed Western blot to compare p53 protein levels between two genotypes. We found that p53 protein was significantly lower in $Hfe^{-/-}$ ileum than in wild-type controls (Figure 7A); the reduction was ∼4-fold compared with the control (Figure 7B). The same was true in $Hfe^{-/-}$ colon (Figure 7C,D).

Effect of p53 reconstitution on FAC-induced decrease in ABCG2 expression

Our studies show that chronic exposure to iron in colonic epithelial cells decreases p53 protein with subsequent decrease in ABCG2 mRNA. To confirm these findings Furthermore, we reconstituted p53 in FAC-exposed cells via ectopic expression to see if it would restore ABCG2 mRNA levels. Initial experiments with FAC-exposed CCD841 cells for ectopic expression of p53 failed due to low transfection efficiency. Therefore, we used HEK293FT cells, which exhibit robust transfection efficiency. We first exposed these cells to FAC (250 μg/ml) for three passages. Control and FAC-exposed cells were then used for transient ectopic expression of p53. FAC was omitted during transfection. We then monitored p53 protein levels (Western blot) and ABCG2 mRNA levels (qRT-PCR) in control and FAC-exposed cells with and without ectopic expression of p53. We observed

Biochemical Journal (2020) **477** 1499–1513
https://doi.org/10.1042/BCJ20190873

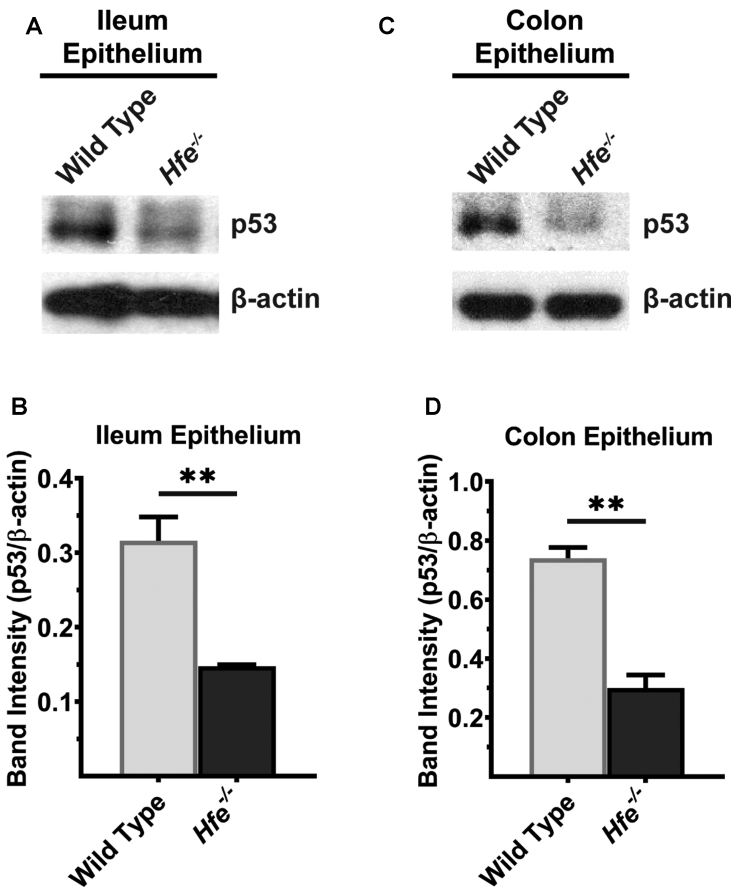

Figure 7. p53 protein levels are significantly decreased in *Hfe*$^{-/-}$ mouse ileum and colonic epithelium.

Western blot for p53 protein in (**A**) ileal and (**C**) colonic epithelium of wild type and *Hfe*$^{-/-}$ mice. Please see Supplementary Figures S13 and S14 for full blot images. Western blot band intensities were estimated using ImageJ software and the band intensities that correspond to p53 protein were normalized to β-actin levels in (**B**) ileal epithelium and (**D**) colonic epithelium. Data represent mean values of three mice per group ± SEM. $^{**}P < 0.01$.

decreased p53 protein in FAC-exposed cells compared with control cells (Supplementary Figure S3A). Under these conditions, we also observed the down-regulation of ABCG2 mRNA (Supplementary Figure S3B). Ectopic expression of p53 reconstituted this protein, both in control and FAC-exposed cells (Supplementary Figure S3A), which led to a significant recovery of ABCG2 mRNA in FAC-exposed cells (Supplementary Figure S3B). These data confirm that the decrease in ABCG2 mRNA in FAC-exposed cells is indeed due to decreased levels of p53 protein.

Discussion

In the present study, we focused on the relationship between hereditary hemochromatosis (HH) and uric acid (UA) homeostasis. The findings and implications of the present study can be summarized as follows (Figure 8). Deletion of the iron-regulatory protein Hfe causes hyperuricemia, and its origin is multifactorial. Under conditions of iron overload as occurs in HH, xanthine oxidase, which generates UA as the final step in the catabolism of purine bases, becomes more active, possibly leading to increased production of UA. In addition, the expression of the UA transporter repertoire changes significantly in the liver and intestinal tract, likely altering transmembrane transport of UA involved in removal of UA from the cells and excretion of UA into intestinal lumen. In our opinion, the most significant finding of the present study is the marked decrease in the expression of the UA exporter Abcg2 in the intestinal tract in HH. This transporter is known to be responsible for ~40% excretion of UA from the body; as such, the decreased expression of this transporter in HH is probably

Biochemical Journal (2020) 477 1499–1513
https://doi.org/10.1042/BCJ20190873

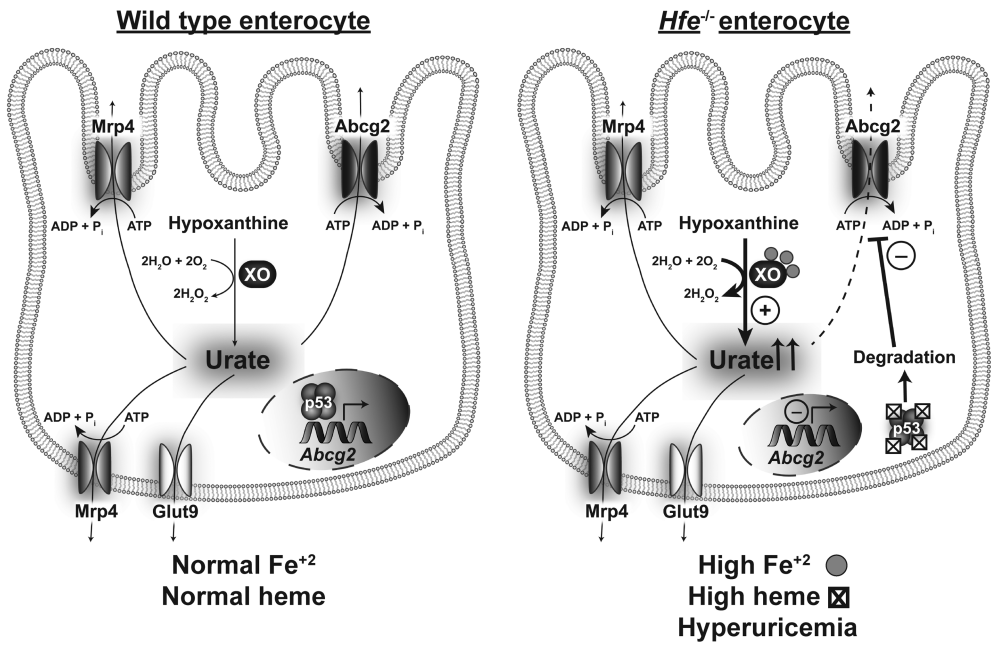

Figure 8. Schematic illustration of the differences in intestinal handling of uric acid between wild type and *Hfe*$^{-/-}$ enterocytes.

the major contributor to HH-associated hyperuricemia. Based on this conclusion, we investigated the molecular events underlying the down-regulation of ABCG2 in HH. We showed that ABCG2 is a direct target for the tumor suppressor p53 and that the protein levels of p53 are profoundly decreased in HH. We have established the regulation of ABCG2 expression by p53 via ChIP that showed binding of p53 to h*ABCG2* gene promoter. We also showed that HH is associated with increased accumulation of heme in epithelial cells lining the ileum and colon; this is relevant to the decrease in p53 protein levels in HH. Studies by others have shown that p53 is a heme-binding protein and that p53-heme complex is a substrate for proteasomal degradation [39]. There is however some discordance between Abcg2 mRNA levels and Abcg2 protein levels in the *Hfe*$^{-/-}$ intestine; the decrease in mRNA is much less pronounced than the decrease in protein. Even though this could be explained by the often observed finding that mRNA levels do not always correspond to protein levels, the possibility of additional transcriptional control of *Abcg2* in HH by factors other than p53 cannot be excluded. The transcription factor Nrf2 is a likely candidate; Nrf2 is known to induce h*ABCG2* transcription [6], and the activity of this transcription factor is increased by oxidative stress as occurs under iron-overload conditions such as HH. Taken collectively, the results of the present study show that hemochromatosis is associated with elevated levels of UA and the iron/heme-p53-ABCG2 axis plays a critical role in this phenomenon. As arthritis is a common pathological symptom in patients with HH, the findings of the current study have profound clinical implications because they underscore the potential involvement of hyperuricemia in the pathogenesis of HH-associated arthropathy.

In contrast with the findings in our study which showed p53 as an inducer of ABCG2 expression, Wang et al. [40] have reported that p53 is a suppressor of ABCG2 expression, not directly but indirectly by decreasing the levels of NFκB. Our studies have shown a direct effect of p53 on ABCG2 expression as documented by the binding of p53 on h*ABCG2* gene promoter. The discrepancy between the two studies is most likely related to potential differences in the expression levels and activity status of NFκB in tissues and cell lines employed.

MRP4 has been shown to be an ATP-dependent urate exporter in a heterologous expression system using HEK293 cells [41]; however, the extent of its involvement in the maintenance of UA homeostasis *in vivo* in humans is not known. Although in experimental animals, knockdown of Mrp4 in kidneys cause reduction in urate export [42], there is no significant association between the *MRP4* gene polymorphism and hyperuricemia and gout occurrence in humans [43]. The only study reported in the literature on any potential association between MRP4 and UA homeostasis is that by Tanner et al. [44]. This study analyzed *MRP4* gene

polymorphism in the settings of hyperuricemia and gout. It was found that amongst the 39 *MRP4* SNPs, only rs4148500 correlated with the hyperuricemia and gout; however, the molecular mechanism for the correlation was not explored. In the present study, we found a dramatic increase in Mrp4 mRNA levels in $Hfe^{-/-}$mouse intestine, but the significance of this finding remains to be investigated. It is possible that the increase in the expression of MRP4 represents an attempt to maintain UA homeostasis as a feedback response to the down-regulation of ABCG2 and the resultant increase UA levels.

To the best of our knowledge, studies by Flais et al. [45] is the only report in published literature that addressed hyperuricemia in HH. These investigators found that in a large cohort of patients who harbored C282Y mutation in HFE, hyperferritinemia (an evidence for iron overload) was associated with hyperuricemia occurrence. Our results are also consistent with the cross-sectional studies conducted in patients with excessive iron accumulation and hyperferritinemia where iron overload was not of a genetic origin as in HH. In these studies, increase in serum ferritin concentrations correlated positively with the increase in UA levels, and the association was independent of gender, race, age, body mass index, and alcohol consumption [46]. The same trend was seen amongst obese adolescents, irrespective of their body mass index [47]. However, these reports did not focus on the causal relationship between iron overload and hyperuricemia. In this regard, the present study is novel, because besides directly demonstrating elevated UA levels in the $Hfe^{-/-}$ mouse model of HH, it provides a molecular mechanism for hyperuricemia in HH.

Does the elevation in UA in HH have a beneficial effect or pathological effect? This question arises because of the dual role of UA, functioning both as an antioxidant and a pro-inflammatory agent. We opine that hyperuricemia in HH is detrimental because of the co-occurrence of free iron. UA is a chelator of iron, and free iron facilitates crystallization of MSU [48]. Besides its deposition in joints, triggering excruciating acute and chronic flares characterized in gout, MSU crystallization is associated with the development of metabolic syndrome [49], cardiovascular diseases [50], liver failure [51], and kidney failure [52]. Occurrence of these maladies is common in HH patients; therefore, our study suggests a plausible connection between hyperuricemia and the aforementioned broad-spectrum of organ dysfunction in HH.

In conclusion, circulating levels of UA are increased significantly in HH, potentially contributing to the known increased incidence of arthritis in this genetic disorder. Our studies uncover at least two molecular mechanisms for this HH-associated hyperuricemia, namely increased generation of UA due to increased enzymatic activity of xanthine oxidase in the liver and intestine, and decreased intestinal excretion of UA due to decreased expression of the UA exporter Abcg2 in the intestinal tract.

Competing Interests

The authors declare that there are no competing interests associated with the manuscript.

Funding

This work was supported by the National Institutes of Health grant R41 AR074854 and the Welch Endowed Chair in Biochemistry, Grant No. BI-0028, at Texas Tech University Health Sciences Center.

Open Access

Open access for this article was enabled by the participation of Texas Tech University Health Sciences Center in an all-inclusive Read & Publish pilot with Portland Press and the Biochemical Society.

Author Contribution

B.R. performed most of the experiments; S.S. and M.N. made significant contribution in some experiments; V.G. designed the study and interpreted the data; V.G. and B.R. wrote the manuscript.

Abbreviations

ChIP, chromatin immunoprecipitation; FAC, ferric ammonium citrate; FBS, fetal bovine serum; HH, hereditary hemochromatosis; MSU, monosodium urate; ROS, reactive oxygen species; UA, uric acid; XO, xanthine oxidase.

References

1 So, A. and Thorens, B. (2010) Uric acid transport and disease. *J. Clin. Invest.* **120**, 1791–1799 https://doi.org/10.1172/JCI42344

2 Fatima, T., McKinney, C., Major, T.J., Stamp, L.K., Dalbeth, N., Iverson, C. et al. (2018) The relationship between ferritin and urate levels and risk of gout. *Arthritis Res. Ther.* **20**, 179 https://doi.org/10.1186/s13075-018-1668-y

Biochemical Journal (2020) **477** 1499–1513
https://doi.org/10.1042/BCJ20190873

3 Desideri, G., Castaldo, G., Lombardi, A., Mussap, M., Testa, A., Pontremoli, R. et al. (2014) Is it time to revise the normal range of serum uric acid levels? *Eur. Rev. Med. Pharmacol. Sci.* **18**, 1295–1306 PMID:24867507
4 So, A.K. and Martinon, F. (2017) Inflammation in gout: mechanisms and therapeutic targets. *Nat. Rev. Rheumatol.* **13**, 639–647 https://doi.org/10.1038/nrrheum.2017.155
5 Desai, J., Steiger, S. and Anders, H.J. (2017) Molecular pathophysiology of gout. *Trends Mol. Med.* **23**, 756–768 https://doi.org/10.1016/j.molmed.2017.06.005
6 Ristic, B., Sikder, O.M.F., Bhutia, Y.D. and Ganapathy, V. (2020) Pharmacologic inducers of the uric acid exporter ABCG2 as potential drugs for treatment of gouty arthritis. *Asian J. Pharm. Sci.* https://doi.org/10.1016/j.ajps.2019.10.002
7 Dabbagh, A.J., Trenam, C.W., Morris, C.J. and Blake, D.R. (1993) Iron in joint inflammation. *Ann. Rheum. Dis.* **52**, 67–73 https://doi.org/10.1136/ard.52.1.67
8 Winterbournn, C.C. (1995) Toxicity of iron and hydrogen peroxide: the Fenton reaction. *Toxicol. Lett.* **82/83**, 969–974 https://doi.org/10.1016/0378-4274(95)03532-X
9 Morris, C.J., Earl, J.R., Trenam, C.W. and Blake, D.R. (1995) Reactive oxygen species and iron–a dangerous partnership in inflammation. *Int. J. Biochem. Cell Biol.* **27**, 109–122 https://doi.org/10.1016/1357-2725(94)00084-0
10 Kra, S.J., Hollingsworth, J.W. and Finch, S.C. (1965) Arthritis with synovial iron deposition in a patient with hemochromatosis. *N. Engl. J. Med.* **272**, 1268–1271 https://doi.org/10.1056/NEJM196506172722404
11 Merryweather-Clarke, A.T., Pointon, J.J., Shearman, J.D. and Robson, K.J.H. (1997) Global prevalence of putative haemochromatosis mutations. *J. Med. Genet.* **34**, 275–278 https://doi.org/10.1136/jmg.34.4.275
12 Adams, P.C. (2015) Epidemiology and diagnostic testing for hemochromatosis and iron overload. *Int. J. Lab. Hem.* **37**, 25–30 https://doi.org/10.1111/ijlh.12347
13 Pietrangelo, A. (2010) Hereditary hemochromatosis: pathogenesis, diagnosis, and treatment. *Gastroenterology* **139**, 393–408 https://doi.org/10.1053/j.gastro.2010.06.013
14 Feder, J.N., Gnirke, A., Thomas, W., Tsuchihashi, Z., Ruddy, D.A., Basava, A. et al. (1996) A novel MHC class I-like gene is mutated in patients with hereditary haemochromatosis. *Nat. Genet.* **13**, 399–408 https://doi.org/10.1038/ng0896-399
15 Wu, X., Wang, Y., Wu, Q., Cheng, W., Liu, W., Zhao, Y. et al. (2014) HFE interacts with the BMP type I receptor ALK3 to regulate hepcidin expression. *Blood* **124**, 1355–1343 https://doi.org/10.1182/blood-2014-01-552281
16 Bridle, K.R., Frazer, D.M., Wilkins, S.J., Dixon, J.L., Purdie, D.M., Crawford, D.H.G. et al. (2003) Disrupted hepcidin regulation in HFE-associated haemochromatosis and the liver as a regulator of body iron homoeostasis. *Lancet* **361**, 669–673 https://doi.org/10.1016/S0140-6736(03)12602-5
17 Nemeth, E., Tuttle, M.S., Powelson, J., Vaughn, M.B., Donovan, A., Ward, D.M. et al. (2004) Hepcidin regulates cellular iron efflux by binding to ferroportin and inducing its internalization. *Science* **306**, 2090–2093 https://doi.org/10.1126/science.1104742
18 Schumacher, Jr, H.R. (1998) Arthropathy in hemochromatosis. *Hosp. Pract. (1995)* **33**, 81–86 https://doi.org/10.1080/21548331.1998.11443654
19 McDonnell, S.M., Preston, B.L., Jewell, S.A., Barton, J.C., Edwards, C.Q., Adams, P.C. et al. (1999) A survey of 2,851 patients with hemochromatosis: symptoms and response to treatment. *Am. J. Med.* **106**, 19–24 https://doi.org/10.1016/S0002-9343(99)00120-5
20 Ross, J.M., Kowalchuk, R.M., Shaulinsky, J., Ross, L., Ryan, D. and Phatak, P.D. (2003) Association of heterozygous hemochromatosis C282Y gene mutation with hand osteoarthritis. *J. Rheumatol.* **30**, 121–125 PMID:12508400
21 Timms, A.E., Sathananthan, R., Bradbury, L., Athanassou, N.A., Wordsworth, B.P. and Brown, M.A. (2002) Genetic testing for haemochromatosis in patients with chondrocalcinosis. *Ann. Rheum. Dis.* **61**, 745–747 https://doi.org/10.1136/ard.61.8.745
22 Willis, G., Scott, D.G., Jennings, B.A., Smith, K., Bukhari, M. and Wimperis, J.Z. (2002) HFE mutations in an inflammatory arthritis population. *Rheumatology (Oxford)* **41**, 176–179 https://doi.org/10.1093/rheumatology/41.2.176
23 Rovetta, G., Grignolo, M.C., Buffrini, L. and Monteforte, P. (2002) Prevalence of C282Y mutation in patients with rheumatoid arthritis and spondylarthritis. *Int. J. Tissue. React.* **24**, 105–109 PMID:12635863
24 Lambert, R.E. (2001) Iron storage diseases. In *Kelley's Textbook of Rheumatology*, 6th edn (Ruddy, S., Harris, E.D. and Sledge, C.B., eds), pp. 1559–1565, WB Saunders, Philadelphia
25 Brighton, C.T., Bigley, Jr, E.C. and Smolenski, B.I. (1970) Iron-induced arthritis in immature rabbits. *Arthritis Rheum.* **13**, 849–857 https://doi.org/10.1002/art.1780130615
26 Bhutia, Y.D., Ogura, J., Grippo, P.J., Torres, C., Sato, T., Wachtel, M. et al. (2020) Chronic exposure to excess iron promotes EMT and cancer via p53 loss in pancreatic cancer. *Asian J. Pharm. Sci.* https://doi.org/10.1016/j.ajps.2020.02.003
27 Kim, J.S., Lee, C., Bonifant, C.L., Ressom, H. and Waldman, T. (2007) Activation of p53-dependent growth suppression in human cells by mutations in PTEN or PIK3CA. *Mol. Cell. Biol.* **27**, 662–677 https://doi.org/10.1128/MCB.00537-06
28 Loughery, J., Cox, M., Smith, L.M. and Meek, D.W. (2014) Critical role for p53-serine 15 phosphorylation in stimulating transactivation at p53-responsive promoters. *Nucleic Acids Res.* **42**, 7666–7680 https://doi.org/10.1093/nar/gku501
29 Kang, D.H., Nakagawa, T., Feng, L., Watanabe, S., Han, L., Mazzali, M. et al. (2002) A role for uric acid in the progression of renal disease. *J. Am. Soc. Nephrol.* **13**, 2888–2897 https://doi.org/10.1097/01.asn.0000034910.58454.fd
30 Kratzer, J.T., Lanaspa, M.A., Murphy, M.N., Cicerchi, C., Graves, C.L., Tipton, P.A. et al. (2014) Evolutionary history and metabolic insights of ancient mammalian uricases. *Proc. Natl Acad. Sci. U.S.A.* **111**, 3763–3768 https://doi.org/10.1073/pnas.1320393111
31 Pritsos, C.A. (2000) Cellular distribution, metabolism and regulation of the xanthine oxidoreductase enzyme system. *Chem. Biol. Interact.* **1**, 195–208 https://doi.org/10.1016/s0009-2797(00)00203-9
32 Okamoto, K., Kusano, T. and Nishino, T. (2013) Chemical nature and reaction mechanisms of the molybdenum cofactor of xanthine oxidoreductase. *Curr. Pharmaceut. Design* **19**, 2606–2614 https://doi.org/10.2174/1381612811319140010
33 Reginato, A.M., Mount, D.B., Yang, I. and Choi, H.K. (2012) The genetics of hyperuricaemia and gout. *Nat. Rev. Rheumatol.* **8**, 610–621 https://doi.org/10.1038/nrrheum.2012.144
34 Hosomi, A., Nakanishi, T., Fujita, T. and Tamai, I. (2012) Extra-renal elimination of uric acid via intestinal efflux transporter BCRP/ABCG2. *PLoS ONE* **7**, e30456 https://doi.org/10.1371/journal.pone.0030456

35 Woodward, O.M., Köttgen, A., Coresh, J., Boerwinkle, E., Guggino, W.B. and Köttgen, M. (2009) Identification of a urate transporter, ABCG2, with a common functional polymorphism causing gout. *Proc. Natl Acad. Sci. U.S.A.* **106**, 10338–10342 https://doi.org/10.1073/pnas.0901249106
36 Nakanishi, T. and Ross, D.D. (2012) Breast cancer resistance protein (BCRP/ABCG2): its role in multidrug resistance and regulation of its gene expression. *Chin. J. Cancer.* **31**, 73–99 https://doi.org/10.5732/cjc.011.10320
37 Nakanishi, T., Bailey-Dell, K.J., Hassel, B.A., Shiozawa, K., Sullivan, D.M., Turner, J. et al. (2006) Novel 5′ untranslated region variants of BCRP mRNA are differentially expressed in drug-selected cancer cells and in normal human tissues: implications for drug resistance, tissue-specific expression, and alternative promoter usage. *Cancer Res.* **66**, 5007–5011 https://doi.org/10.1158/0008-5472.CAN-05-4572
38 Zong, Y., Zhou, S., Fatima, S. and Sorrentino, B.P. (2006) Expression of mouse Abcg2 mRNA during hematopoiesis is regulated by alternative use of multiple leader exons and promoters. *J. Biol. Chem.* **281**, 29625–29632 https://doi.org/10.1074/jbc.M606314200
39 Shen, J., Sheng, X., Chang, Z., Wu, Q., Wang, S., Xuan, Z. et al. (2014) Iron metabolism regulates p53 signaling through direct heme-p53 interaction and modulation of p53 localization, stability, and function. *Cell Rep.* **7**, 180–193 https://doi.org/10.1016/j.celrep.2014.02.042
40 Wang, X., Wu, X., Wang, C., Zhang, W., Ouyang, Y., Yu, Y. et al. (2010) Transcriptional suppression of breast cancer resistance protein (BCRP) by wild-type p53 through the NF-kappaB pathway in MCF-7 cells. *FEBS Lett.* **584**, 3392–3397 https://doi.org/10.1016/j.febslet.2010.06.033
41 Van Aubel, R.A., Smeets, P.H., van den Heuvel, J.J. and Russel, F.G. (2005) Human organic anion transporter MRP4 (ABCC4) is an efflux pump for the purine end metabolite urate with multiple allosteric substrate binding sites. *Am. J. Physiol. Renal. Physiol.* **288**, F327–F333 https://doi.org/10.1152/ajprenal.00133.2004
42 Bataille, A.M., Goldmeyer, J. and Renfro, J.L. (2008) Avian renal proximal tubule epithelium urate secretion is mediated by Mrp4. *Am. J. Physiol. Regul. Integr. Comp. Physiol.* **295**, R2024–R2033 https://doi.org/10.1152/ajpregu.90471.2008
43 Bobulescu, I.A. and Moe, O.W. (2012) Renal transport of uric acid: evolving concepts and uncertainties. *Adv. Chronic Kidney Dis.* **19**, 358–371 https://doi.org/10.1053/j.ackd.2012.07.009
44 Tanner, C., Boocock, J., Stahl, E.A., Dobbyn, A., Mandal, A.K. and Cadzow, M. (2017) Population specific resequencing associates the ATP binding cassette subfamily C member 4 (ABCC4) gene with gout in New Zealand Māori and Pacific men. *Arthritis Rheumatol.* **69**, 1461–1469 https://doi.org/10.1002/art.40110
45 Flais, J., Bardou-Jacquet, E., Deugnier, Y., Coiffier, G., Perdriger, A., Chalès, G. et al. (2017) Hyperferritinemia increases the risk of hyperuricemia in HFE-hereditary hemochromatosis. *Joint Bone Spine* **84**, 293–297 https://doi.org/10.1016/j.jbspin.2016.05.020
46 Ghio, A.J., Ford, E.S., Kennedy, T.P. and Hoidal, J.R. (2005) The association between serum ferritin and uric acid in humans. *Free Radic. Res.* **39**, 337–342 https://doi.org/10.1080/10715760400026088
47 Chen, S.C.C., Huang, Y.F. and Wang, J.D. (2012) Hyperferritinemia and hyperuricemia may be associated with liver function abnormality in obese adolescents. *PLoS ONE* **7**, e48645 https://doi.org/10.1371/journal.pone.0048645
48 Ghio, A.J., Kennedy, T.P., Rao, G., Cooke, C.L., Miller, M.J. and Hoidal, J.R. (1994) Complexation of iron cation by sodium urate crystals and gouty inflammation. *Arch. Biochem. Biophys.* **313**, 215–221 https://doi.org/10.1006/abbi.1994.1379
49 DeBosch, B.J., Kluth, O., Fujiwara, H., Schürmann, A. and Moley, K. (2014) Early-onset metabolic syndrome in mice lacking the intestinal uric acid transporter SLC2A9. *Nat. Commun.* **7**, 4642 https://doi.org/10.1038/ncomms5642
50 Wang, H., Zhang, H., Sun, L. and Guo, W. (2018) Roles of hyperuricemia in metabolic syndrome and cardiac-kidney-vascular system diseases. *Am. J. Transl. Res.* **10**, 2749–2763 PMID:30323864
51 Oh, T.R., Choi, H.S., Kim, C.S., Bae, E.H., Ma, S.K., Sung, S.A. et al. (2019) Hyperuricemia has increased the risk of progression of chronic kidney disease: propensity score matching analysis from the KNOW-CKD study. *Sci. Rep.* **30**, 6681 https://doi.org/10.1038/s41598-019-43241-3
52 Li, Y., Xu, C., Yu, C., Xu, L. and Miao, M. (2009) Association of serum uric acid level with non-alcoholic fatty liver disease: a cross-sectional study. *J. Hepatol.* **50**, 1029–1034 https://doi.org/10.1016/j.jhep.2008.11.021

Supplementary Information

Supplementary Table S1. Sequences of PCR Primers used in this study.

Target	Primer Sequence (5'-3')
mXO	ATG GCA AAA AGG TGG TGG AGA
	GCA ACA TGA TGC AAG GAG CA
mGlut9	TGC ATT GGC GTG TTT TCT GG
	AAA GAG AAG GTA GCG TGG GC
mMrp4	TCT GCG AGC CAA GAA GGA CT
	TCG TCG GGG TCA TAC TTC TCA
mAbcg2	ATA GCC ACA GGC CAA AGT GT
	ACT GCA AAG CTG TGA AGC CA
***hABCG2* ChIP primer**	GAG CAG CGC TTG TGA CTG G
	ACA CGC AGG GAC AAG CCA AA
***hP21* ChIP primer**	CCC ACA GCA GAG GAG AAA GAA
	CTG GAA ATC TCT GCC CAG ACA
***hGADD45A* ChIP Primer**	TCC GAC TAG AGT GTG GCT GG
	ATG AGG GGT GAG CCA GGA AT
***hGAPDH* ChIP Primer**	TAC TAG CGG TTT TAC GGG CG
	TCG AAC AGG AGG AGC AGA GAG CGA
mUrate Oxidase	GTG AGC ACT TCC TCT CTT CTT T
	GGA CGT GTT TGA TCC CAT TCT
m/hHPRT	GCG TCG TGA TTA GCG ATG ATG AAC
	CCT CCC ATC TCC TTC ATG ACA TCT
mGAPDH	TGT AGA CCA TGT AGT TGA GGT CA
	AGG TCG GTG TGA ACG GAT TTG
hABCG2	TCA GAT GGG TTT CCA AGC GT
	AAC CCC AGC TCT GTT CTG GA

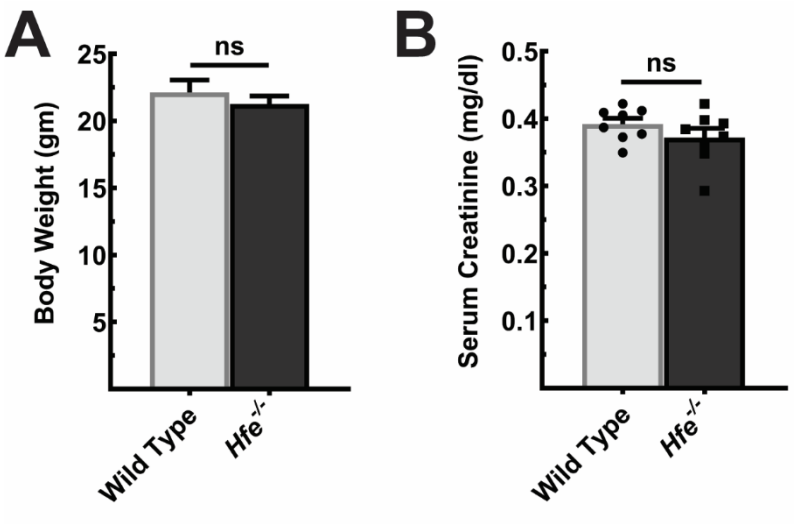

Supplementary Figure S1. Serum creatinine levels as a surrogate for glomerular filtration rate in *Hfe*$^{-/-}$ mouse. (**A**) Body weight for *Hfe*$^{-/-}$ mice and wild type control mice at the time of serum collection. Data show mean ± SEM for 4 mice (all males) per group. ns, not significant. (**B**) Serum creatinine levels were measured in *Hfe*$^{-/-}$ mice and wild type counterparts using Creatinine Assay Kit. Data show mean ± SEM for 4 mice per group. ns, not significant.

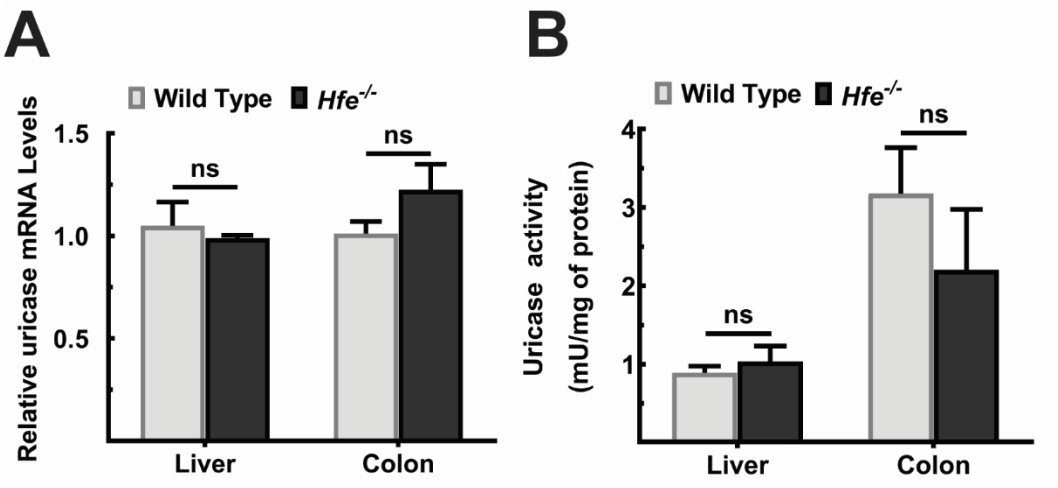

Supplementary Figure S2. Expression and activity of uricase in wild type and *Hfe*$^{-/-}$ mouse liver and colon. (**A**) Quantitative PCR analysis of uricase mRNA in liver and colon of *Hfe*$^{-/-}$ and wild type mice. Data show mean ± SEM for 3 mice per group. ns, not significant. (**B**) Uricase activity in wild type and *Hfe*$^{-/-}$ mice as assessed by the Amplex® Red Uric Acid/Uricase Assay Kit. Data show the mean ± SEM for 3 mice per group. ns, not significant.

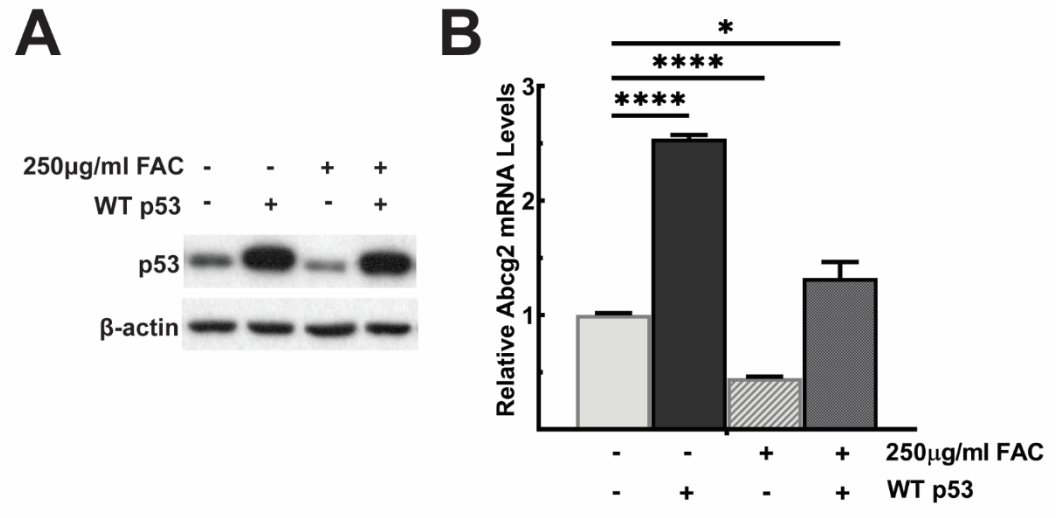

Supplementary Figure S3. ABCG2 expression levels upon iron-induced p53 degradation and subsequent ectopic overexpression of p53. HEK293FT cells were chronically treated with 250 µg/ml FAC for three passages to mimic the environment of the chronic exposure to excess iron. Cells then underwent transfection with pcDNA3-p53 or empty pcDNA3 plasmid constructs. FAC was omitted during transfection. Cells were then used for preparation of protein lysates and total RNA. (**A**) Western blot for p53 protein levels. (**B**) Quantitative PCR analysis to assess ABCG2 mRNA levels. Data show mean ± SEM for 3 independent experiments. *$P < 0.05$; ****$P < 0.0001$.

Raw Western Blots

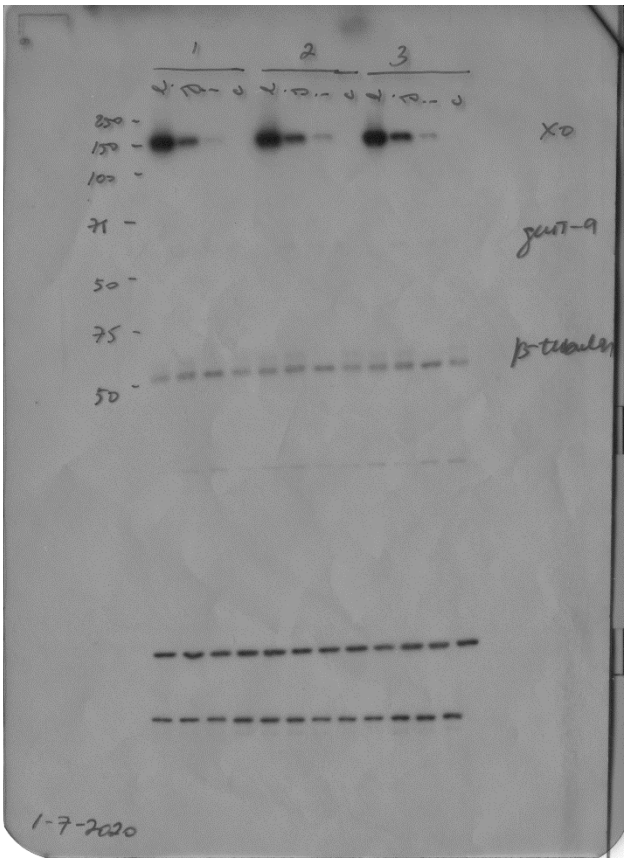

Supplementary Figure S4. Rows from the top: (**1**) XO in WT Liver, Jejunum, Ileum and Colon. Used in Figure 2B. The rest not used. Please disregard.

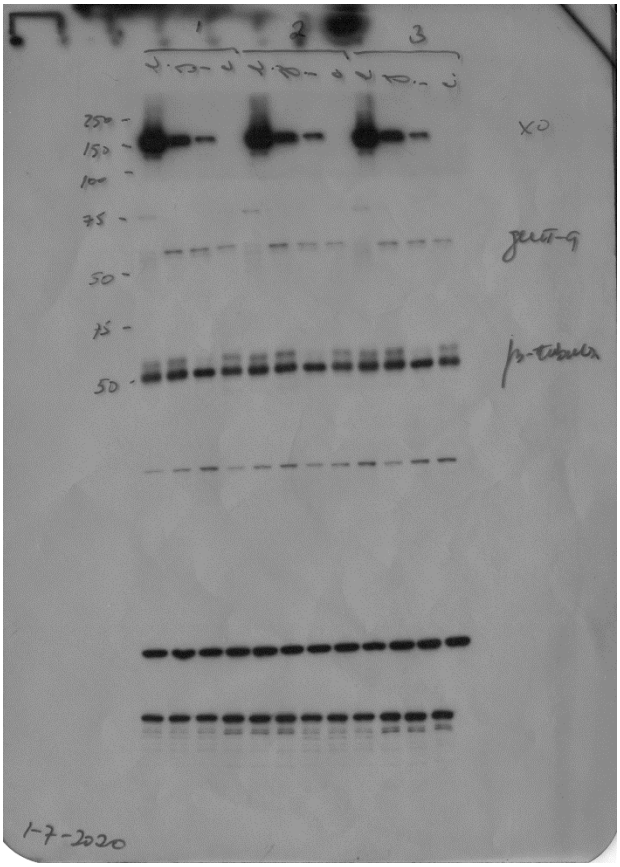

Supplementary Figure S5. Rows from the top: (**1**) XO in WT Liver, Jejunum, Ileum and Colon, longer exposure; (**2**) Not used. Please disregard; (**3**) β-tubulin in WT Liver, Jejunum, Ileum and Colon. Used in Figures 2B and 3B. The rest not used. Please disregard.

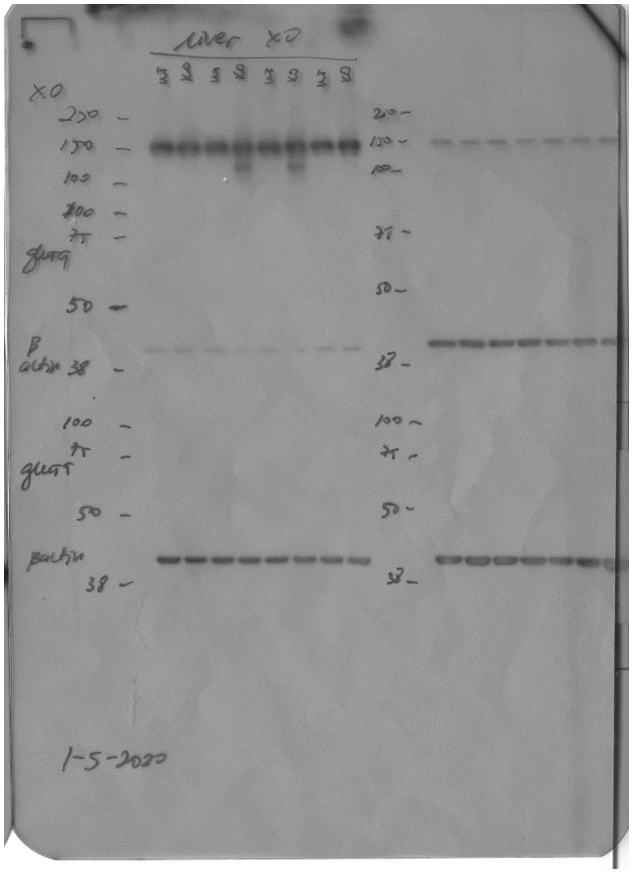

Supplementary Figure S6. Top left row: XO in WT (lanes 1,3,5,7) and *Hfe*$^{-/-}$ (lanes 2,4,6,8) liver. Used in Figure 2D. The rest not used. Please disregard.

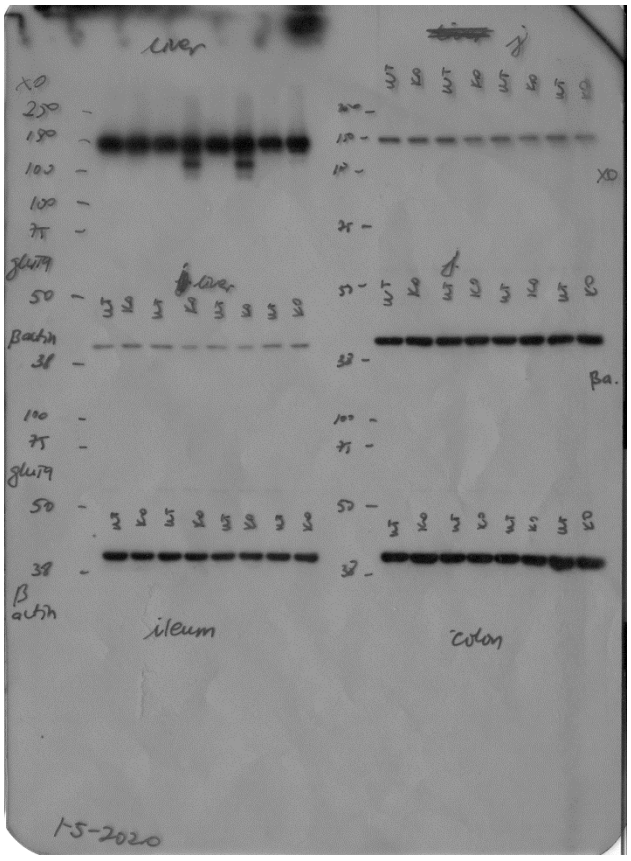

Supplementary Figure S7. Top right row: XO in WT (lanes 1,3,5,7) and *Hfe*$^{-/-}$ (lanes 2,4,6,8) jejunum. Used in Figure 2D. The rest not used. Please disregard.

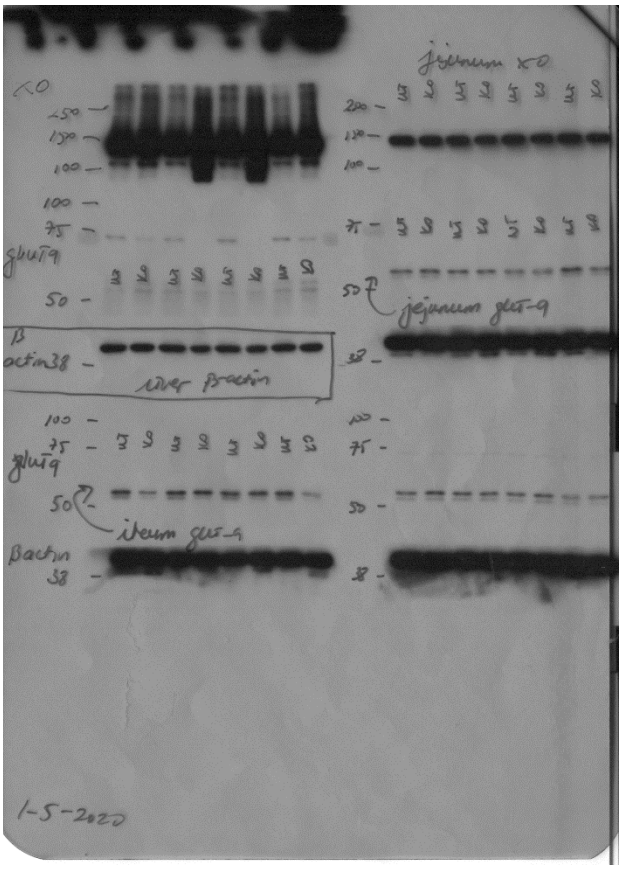

Supplementary Figure S8. Middle right row: β-actin in WT (lanes 1,3,5,7) and *Hfe*$^{-/-}$ (lanes 2,4,6,8) liver. Used in Figures 2D and 3D. The rest not used. Please disregard.

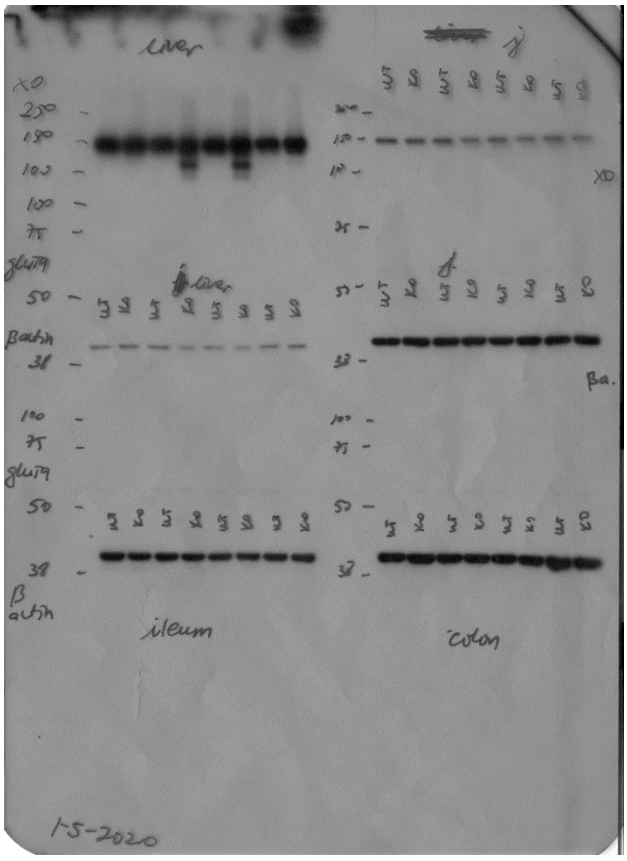

Supplementary Figure S9. Left side, rows from the top: (**1**) XO in WT (lanes 1,3,5,7) and *Hfe*$^{-/-}$ (lanes 2,4,6,8) liver. Higher exposure. (**2**) β-actin in WT (lanes 1,3,5,7) and *Hfe*$^{-/-}$ (lanes 2,4,6,8) liver. Lower exposure; (**3**) β-actin in WT (lanes 1,3,5,7) and *Hfe*$^{-/-}$ (lanes 2,4,6,8) ileum. Used in Figure 3D. Right side, rows from the top: (**1**) XO in WT (lanes 1,3,5,7) and *Hfe*$^{-/-}$ (lanes 2,4,6,8) jejunum; (**2**) β-actin in WT (lanes 1,3,5,7) and *Hfe*$^{-/-}$ (lanes 2,4,6,8) jejunum. Used in Figures 2D and 3D; (**3**) β-actin in WT (lanes 1,3,5,7) and *Hfe*$^{-/-}$ (lanes 2,4,6,8) colon. Used in Figure 3D.

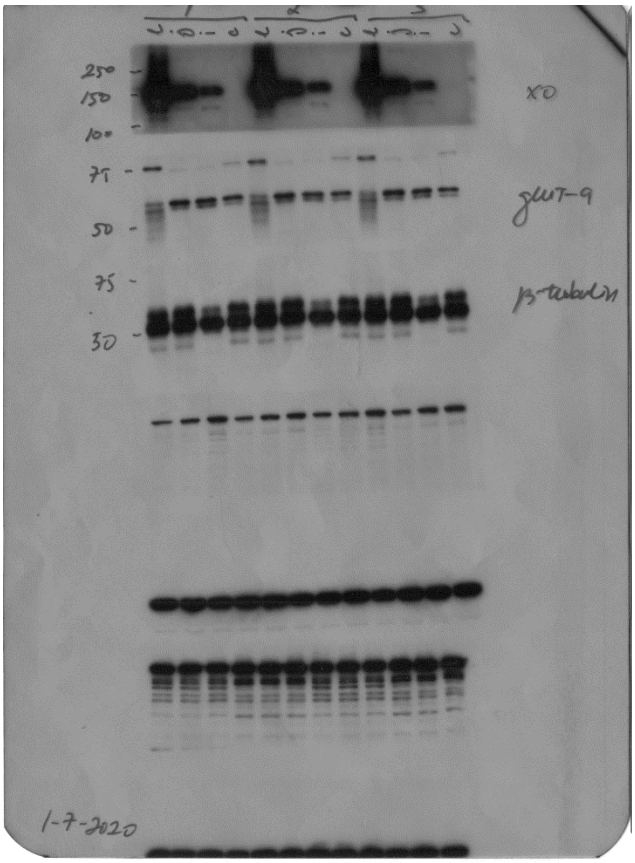

Supplementary Figure S10. Rows from the top: (**1**) XO in WT Liver, Jejunum, Ileum and Colon. Not used. (**2**) Glut9 in WT Liver, Jejunum, Ileum and Colon. Used in Figure 3B. The rest not used. Please disregard.

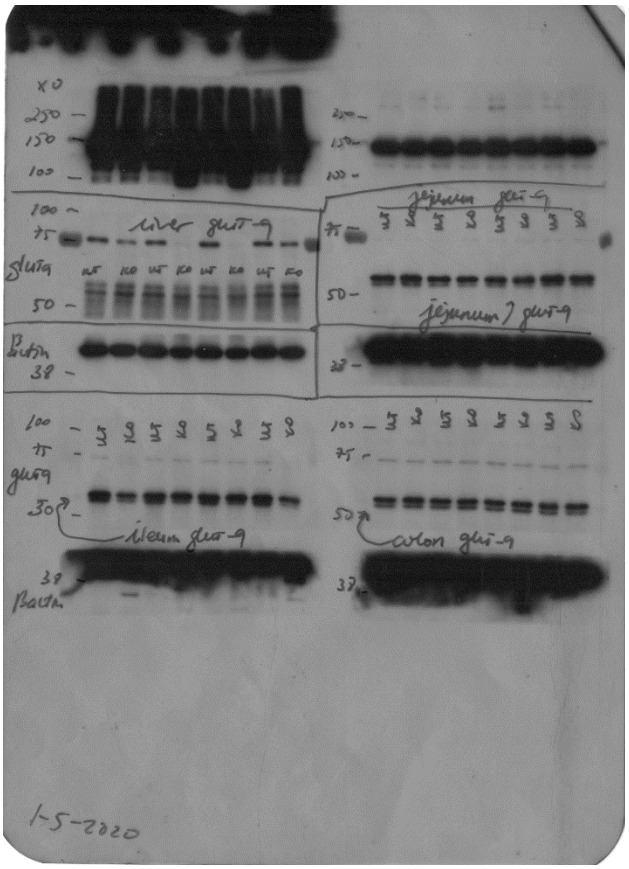

Supplementary Figure S11. Left side, rows from the top: (**1**) Not used, please disregard; (**2**) Glut9 in WT (lanes 1,3,5,7) and *Hfe*$^{-/-}$ (lanes 2,4,6,8) liver. Used in Figure 3D; (**3**) Not used. Please disregard; (**4**) Glut9 in WT (lanes 1,3,5,7) and *Hfe*$^{-/-}$ (lanes 2,4,6,8) ileum. Used in Figure 3D; (**4**) Not used. Please disregard. Right side, rows from the top: (**1**) Not used, please disregard; (**2**) Glut9 in WT (lanes 1,3,5,7) and *Hfe*$^{-/-}$ (lanes 2,4,6,8) jejunum. Used in Figure 3D; (**3**) Not used. Please disregard; (**4**) Glut9 in WT (lanes 1,3,5,7) and *Hfe*$^{-/-}$ (lanes 2,4,6,8) colon. Used in Figure 3D; (**4**) Not used. Please disregard.

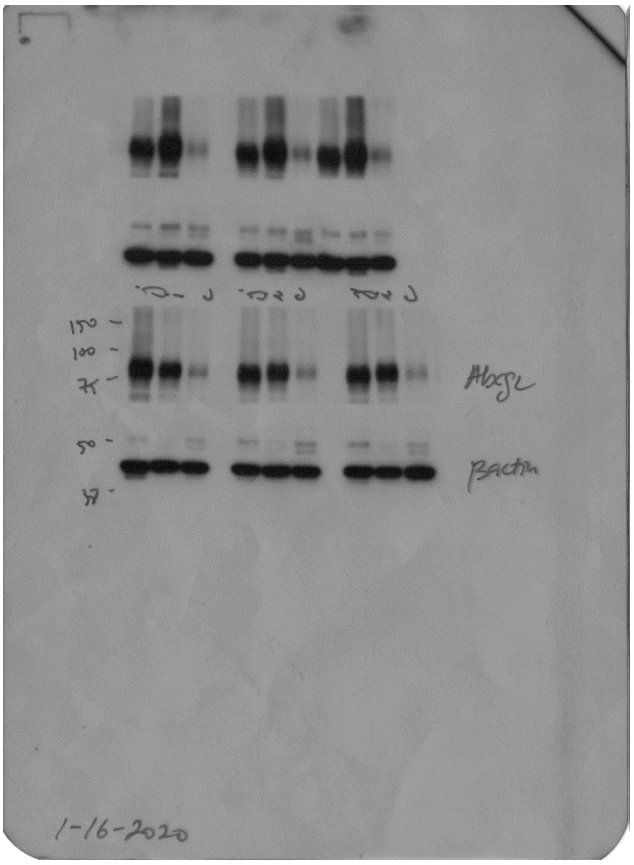

Supplementary Figure S12. Rows from the top: (**1**) and (**2**) Not used. Please disregard; (**3**) Abcg2 in jejunum, ileum and colon epithelium, in triplicates. Used in Figure 4B; (**4**) β-actin in jejunum, ileum and colon epithelium, in triplicates. Used in Figure 4B.

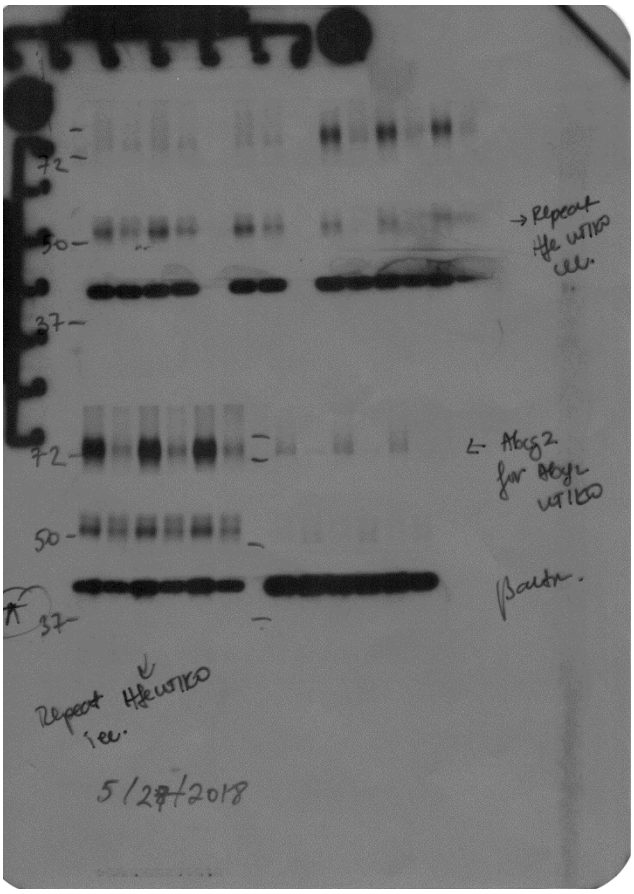

Supplementary Figure S13. Rows from the top: (**1**) Only last 6 lanes used. Abcg2 in WT (lanes 9,11,13) and *Hfe*$^{-/-}$ (lanes 10,12,14) colon epithelium. Used in Figure 5B; (**2**) Only first 7 lanes used (lane 5 is blank). p53 in WT (lanes 1,3,6) and *Hfe*$^{-/-}$ (lanes 2,4,7) colon epithelium. Used in Figure 7C; (**3**) β-actin in WT (lanes 1,3,6,9,11,13) and *Hfe*$^{-/-}$ (lanes 2,4,7,10,12,14) colon epithelium. Used in Figures 5B and 7C; (**4**) Only first 6 lanes used. Abcg2 in WT (lanes 1,3,5) and *Hfe*$^{-/-}$ (lanes 2,4,6) ileum epithelium. Used in Figure 5B; (**5**) Only first 6 lanes used. p53 in WT (lanes 1,3,5) and *Hfe*$^{-/-}$ (lanes 2,4,6) ileum epithelium. Used in Figure 7A; (**6**) Only first 6 lanes used. β-actin in WT (lanes 1,3,5) and *Hfe*$^{-/-}$ (lanes 2,4,6) ileum epithelium. Used in Figures 5B and 7A. Please disregard the rest.

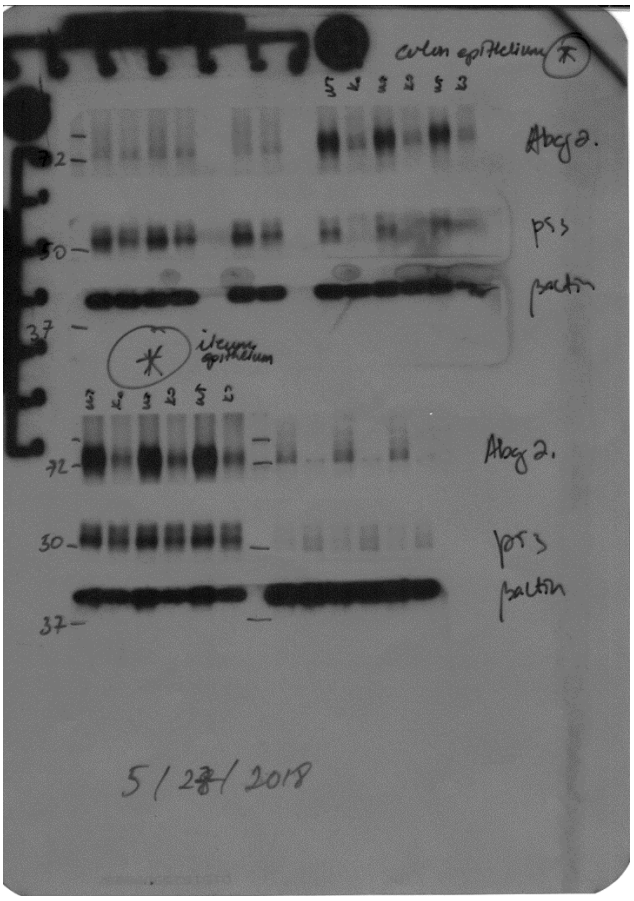

Supplementary Figure S14. Higher exposure of Supplementary Figure S13. Rows from the top: (**1**) Only last 6 lanes used. Abcg2 in WT (lanes 9,11,13) and *Hfe*$^{-/-}$ (lanes 10,12,14) colon epithelium. Used in Figure 5B; (**2**) Only first 7 lanes used (lane 5 is blank). p53 in WT (lanes 1,3,6) and *Hfe*$^{-/-}$ (lanes 2,4,7) colon epithelium. Used in Figure 7C; (**3**) β-actin in WT (lanes 1,3,6,9,11,13) and *Hfe*$^{-/-}$ (lanes 2,4,7,10,12,14) colon epithelium. Used in Figures 5B and 7C; (**4**) Only first 6 lanes used. Abcg2 in WT (lanes 1,3,5) and *Hfe*$^{-/-}$ (lanes 2,4,6) ileum epithelium. Used in Figure 5B; (**5**) Only first 6 lanes used. p53 in WT (lanes 1,3,5) and *Hfe*$^{-/-}$ (lanes 2,4,6) ileum epithelium. Used in Figure 7A; (**6**) Only first 6 lanes used. β-actin in WT (lanes 1,3,5) and *Hfe*$^{-/-}$ (lanes 2,4,6) ileum epithelium. Used in Figures 5B and 7A. Please disregard the rest.

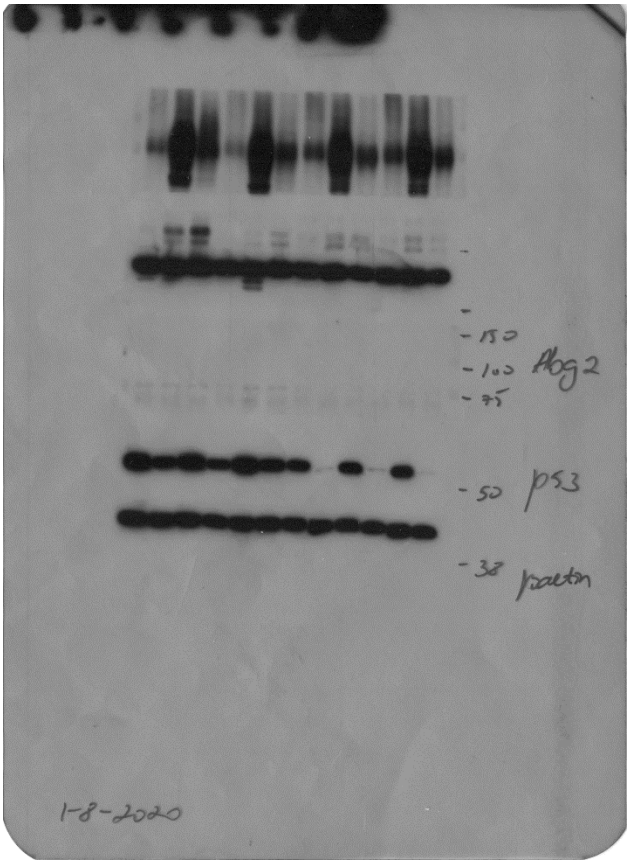

Supplementary Figure S15. Rows from the top: (**1**), (**2**), and (**3**) Not used. Please disregard; (**4**) Only last 6 lanes used. p53 in CCD841 pLKO.1 (lanes 7, 9, and 11) and p53 shRNA (lanes 8, 10, and 12). Used in Figure 6B; (**5**) Not used. Please disregard.

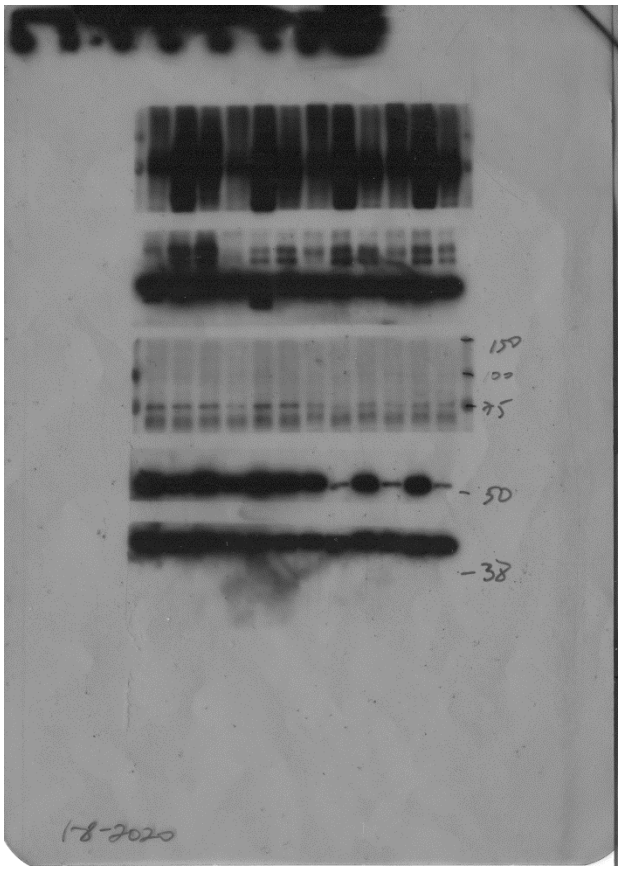

Supplementary Figure S16. Higher exposure of Supplementary Figure S15. Rows from the top: (**1**) and (**2**) Not used. Please disregard; (**3**) Only last 6 lanes used. ABCG2 in CCD841 pLKO.1 (lanes 7, 9, and 11) and p53 shRNA (lanes 8, 10, and 12). Used in Figure 6B; (**4**) and (**5**) Not used. Please disregard.

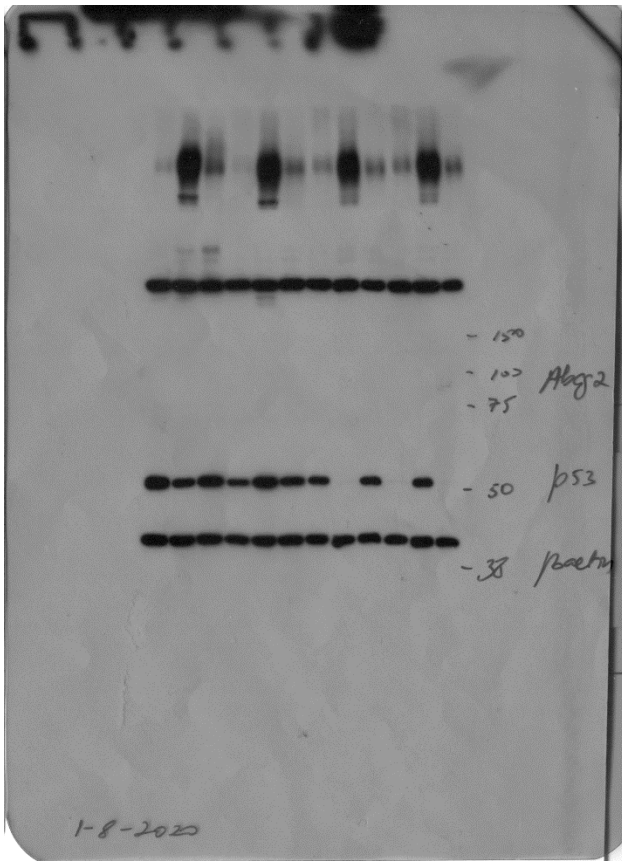

Supplementary Figure S17. Lower exposure of Supplementary Figure S15. Only last row used. Please disregard the rest. (**5**) Only last 6 lanes used. β-actin in CCD841 pLKO.1 (lanes 7, 9, and 11) and p53 shRNA (lanes 8, 10, and 12). Used in Figure 6B.

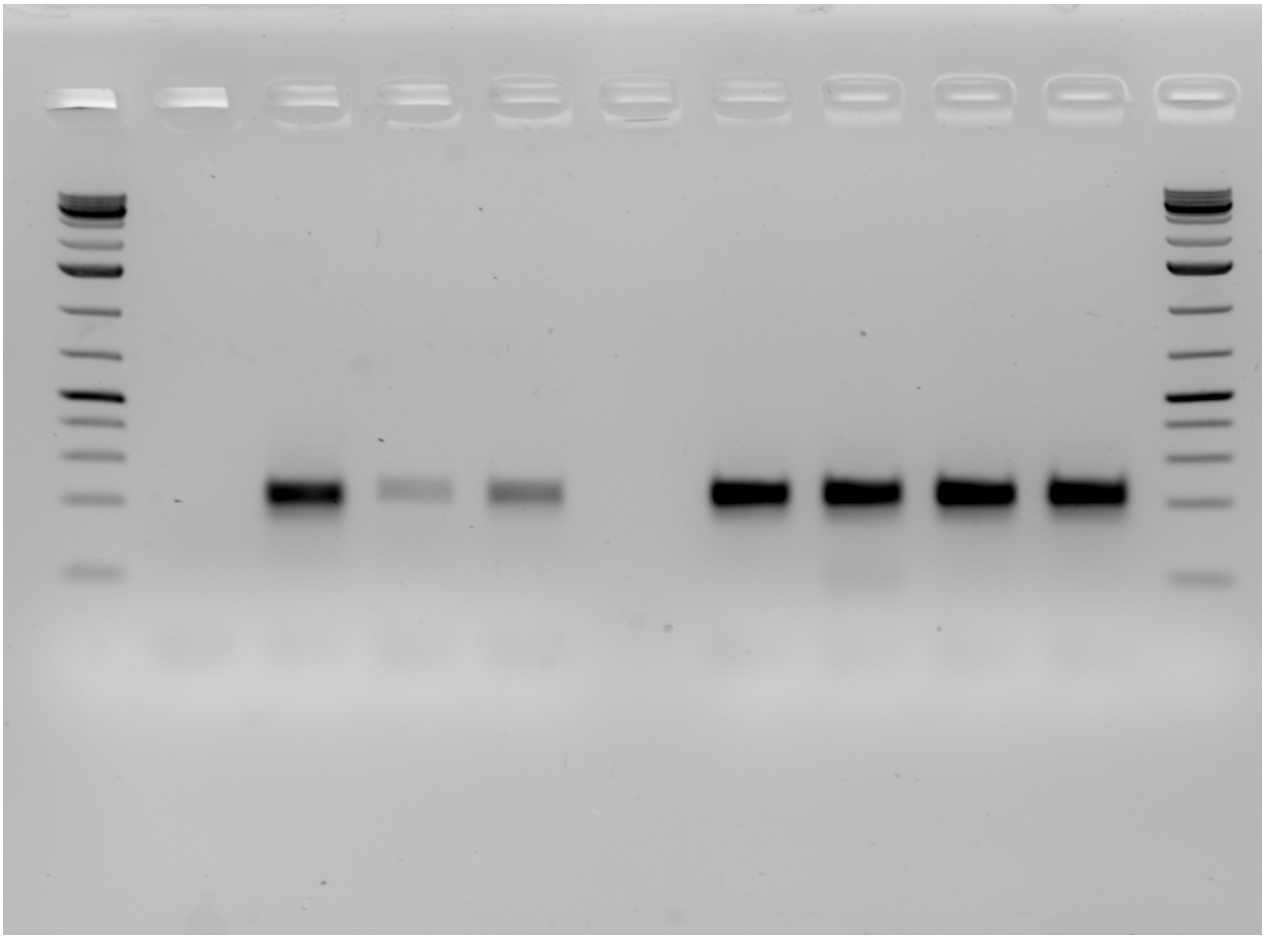

Supplementary Figure S18. Agarose gel for ChIP *ABCG2*. First 4 lanes are pulldown. Last 4 lanes are the input. Lanes 1,3,6,8 are the IgG. Lanes 2,4,7,9 are p53 IP. Lanes 1,2,6,7 are CCD841 pLKO.1. Lanes 3,4,8,9 are CCD841 p53 shRNA. Used in Figure 6B.

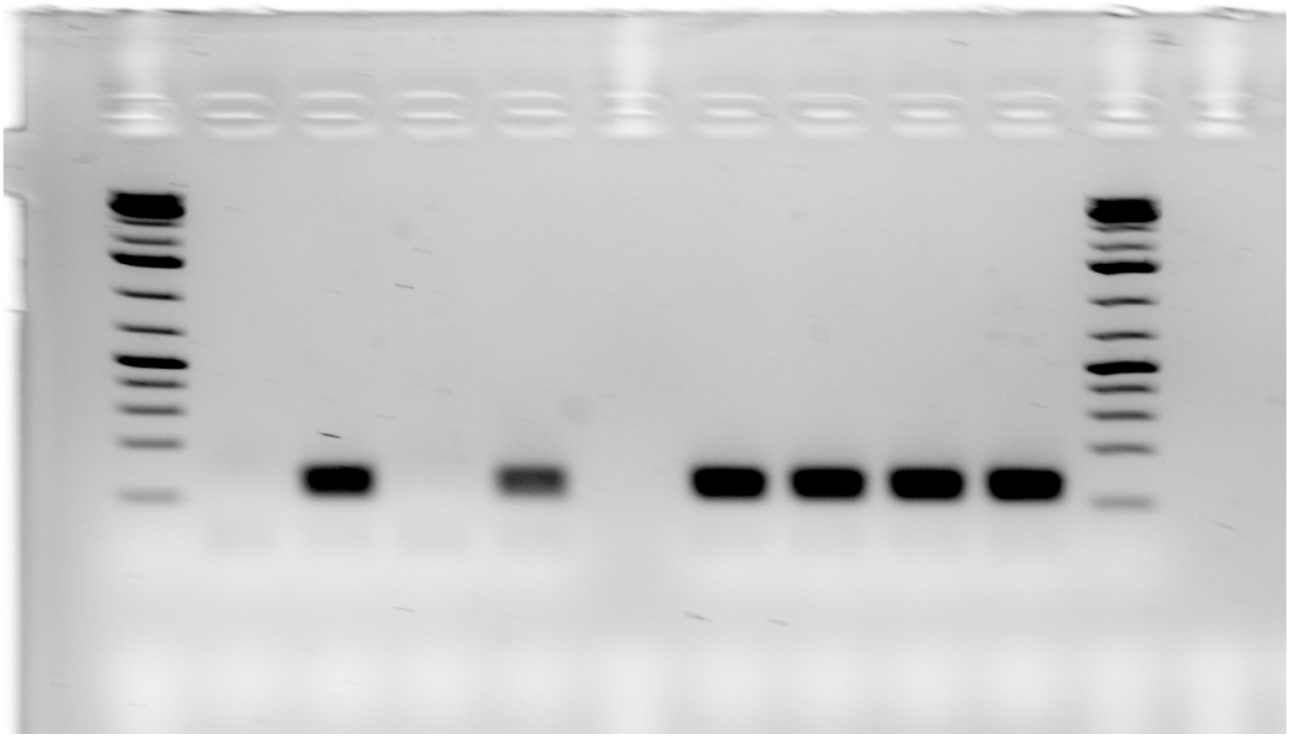

Supplementary Figure S19. Agarose gel of ChIP *p21*. First 4 lanes are pulldown. Last 4 lanes are the input. Lanes 1,3,6,8 are the IgG. Lanes 2,4,7,9 are p53 IP. Lanes 1,2,6,7 are CCD841 pLKO.1. Lanes 3,4,8,9 are CCD841 p53 shRNA. Used in Figure 6B.

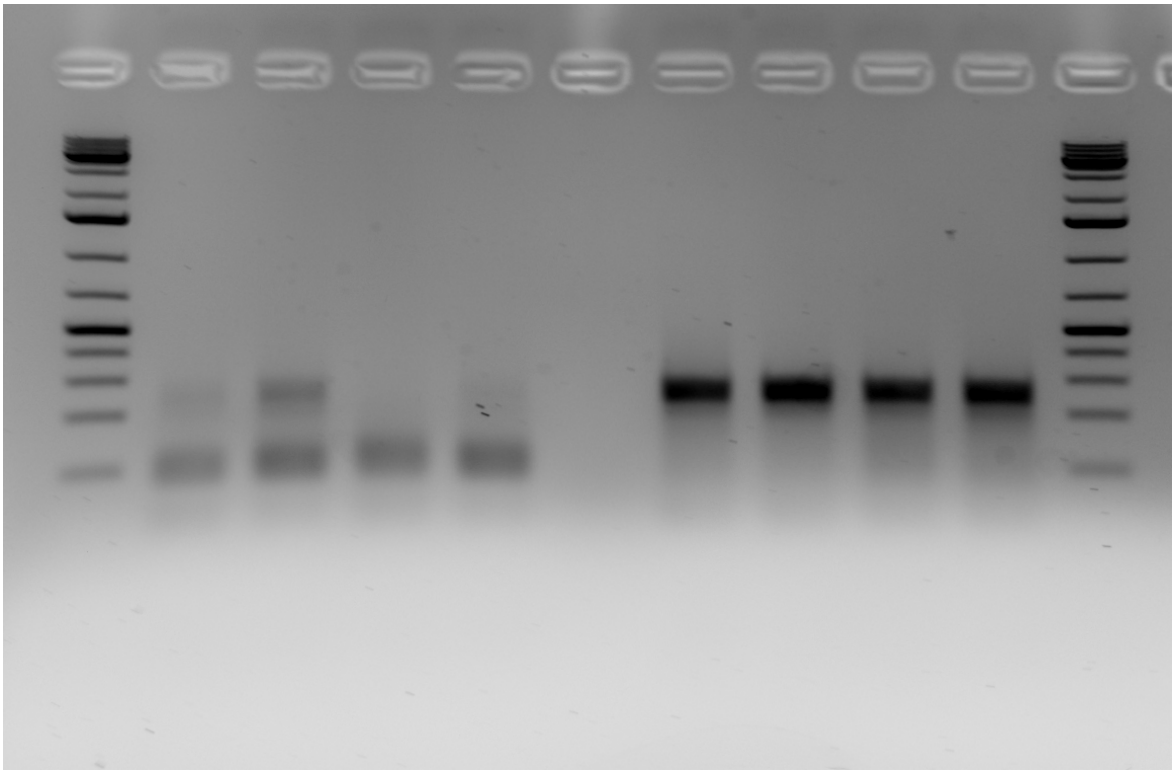

Supplementary Figure S20. Agarose gel of ChIP *GADD45A*. First 4 lanes are pulldown. Last 4 lanes are the input. Lanes 1,3,6,8 are the IgG. Lanes 2,4,7,9 are p53 IP. Lanes 1,2,6,7 are CCD841 pLKO.1. Lanes 3,4,8,9 are CCD841 p53 shRNA. Used in Figure 6B.

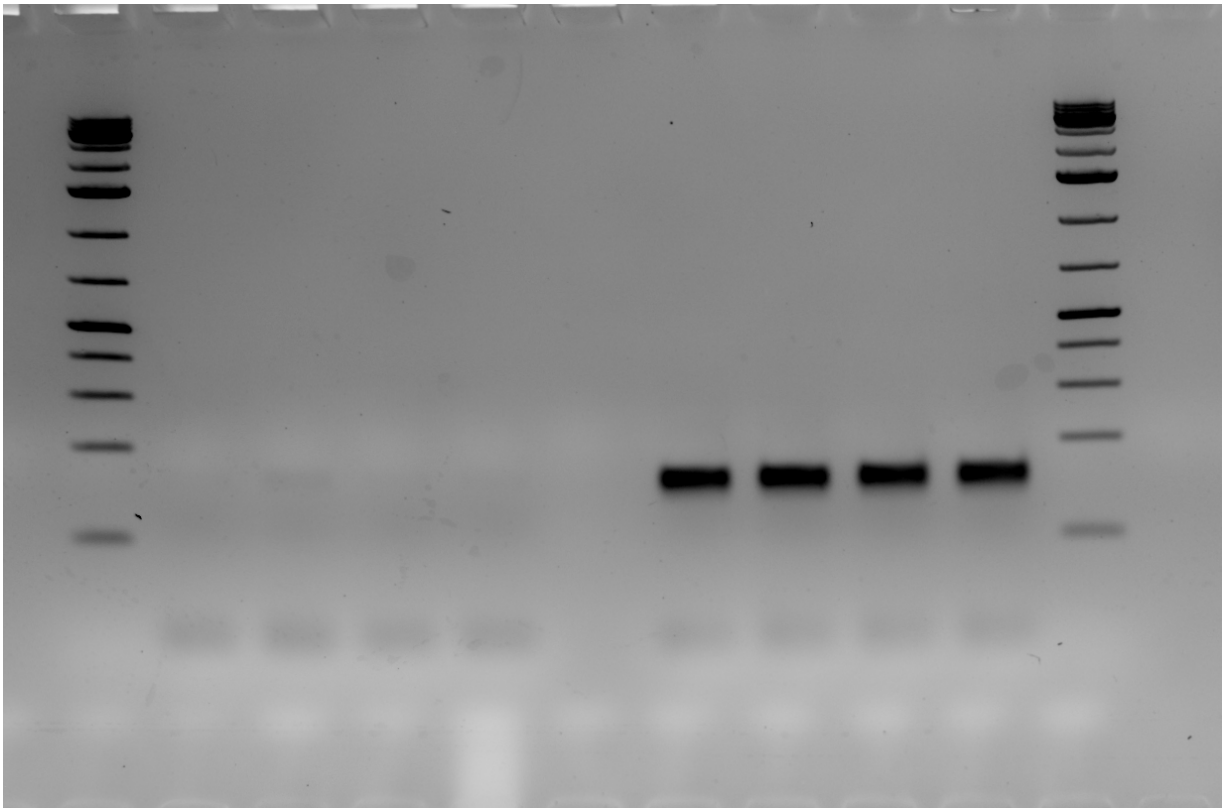

Supplementary Figure S21. Agarose gel of ChIP *GAPDH.* First 4 lanes are pulldown. Last 4 lanes are the input. Lanes 1,3,6,8 are the IgG. Lanes 2,4,7,9 are p53 IP. Lanes 1,2,6,7 are CCD841 pLKO.1. Lanes 3,4,8,9 are CCD841 p53 shRNA. Used in Figure 6B.